ORNL/TM-2022/2354

WIRE-21 Sensor Irradiation Experiment Ready for HFIR Insertion

Christian M. Petrie
Austin S. Chapel
Padhraic L. Mulligan
David Bryant
Daniel C. Sweeney
Adam James
N. Dianne B. Ezell
Kurt Smith
Kara Godsey
Maureen Searles
Shawn Stafford
Jeff Arndt
Jorge Carvajal

Approved for public release.
Distribution is unlimited.

February 2022

OAK RIDGE National Laboratory

ORNL IS MANAGED BY UT-BATTELLE LLC FOR THE US DEPARTMENT OF ENERGY

DOCUMENT AVAILABILITY

Reports produced after January 1, 1996, are generally available free via OSTI.GOV.

Website www.osti.gov

Reports produced before January 1, 1996, may be purchased by members of the public from the following source:

National Technical Information Service
5285 Port Royal Road
Springfield, VA 22161
Telephone 703-605-6000 (1-800-553-6847)
TDD 703-487-4639
Fax 703-605-6900
E-mail info@ntis.gov
Website http://classic.ntis.gov/

Reports are available to US Department of Energy (DOE) employees, DOE contractors, Energy Technology Data Exchange representatives, and International Nuclear Information System representatives from the following source:

Office of Scientific and Technical Information
PO Box 62
Oak Ridge, TN 37831
Telephone 865-576-8401
Fax 865-576-5728
E-mail reports@osti.gov
Website https://www.osti.gov/

This report was prepared as an account of work sponsored by an agency of the United States Government. Neither the United States Government nor any agency thereof, nor any of their employees, makes any warranty, express or implied, or assumes any legal liability or responsibility for the accuracy, completeness, or usefulness of any information, apparatus, product, or process disclosed, or represents that its use would not infringe privately owned rights. Reference herein to any specific commercial product, process, or service by trade name, trademark, manufacturer, or otherwise, does not necessarily constitute or imply its endorsement, recommendation, or favoring by the United States Government or any agency thereof. The views and opinions of authors expressed herein do not necessarily state or reflect those of the United States Government or any agency thereof.

ORNL/TM-2022/2354

Nuclear Science User Facilities Program

WIRE-21 SENSOR IRRADIATION EXPERIMENT READY FOR HFIR INSERTION

Christian M. Petrie
Austin S. Chapel
Padhraic L. Mulligan
David Bryant
Daniel C. Sweeney
Adam James
N. Dianne B. Ezell
Kurt Smith
Kara Godsey
Maureen Searles
Shawn Stafford
Jeff Arndt
Jorge Carvajal

February 2022

Milestone #: M3UF-21OR0212143

Prepared by
OAK RIDGE NATIONAL LABORATORY
Oak Ridge, TN 37831
managed by
UT-BATTELLE LLC
for the
US DEPARTMENT OF ENERGY
under contract DE-AC05-00OR22725

CONTENTS

LIST OF FIGURES

LIST OF TABLES

ACKNOWLEDGMENTS

This research was sponsored by the Nuclear Science User Facilities Program of the US Department of Energy (DOE) Office of Nuclear Energy. The report was authored by UT-Battelle under contract no. DE-AC05-00OR22725 with DOE. Kory Linton served as the program manager for this award, which is led by Westinghouse Electric Company. Bob Sitterson of Oak Ridge National Laboratory (ORNL) assisted with the experiment assembly. Dillon Inabinett and Leonard Mostella of ORNL provided input on experiment cabling and gas line connections.

ABSTRACT

The ability to deploy new nuclear fuels for current or future reactor concepts requires a wealth of data regarding fuel performance during normal operation, anticipated operational occurrences, and design-basis accidents. Most of these data have historically been collected during experiments in materials test reactors, ideally with online instrumentation to collect as much data as possible. However, advanced instrumentation could also allow for in situ monitoring of fuel operating conditions during commercial reactor operation to maximize fuel utilization, reduce unnecessary conservativism in design margins, and improve operator understanding of limiting peaking factors. The latter approach would complicate fuel handling, particularly during refueling, unless the instrumentation could be placed inside the fuel rods and transmitted wirelessly to a receiver located outside the fuel's primary pressure boundary. To this end, Westinghouse Electric Company (WEC) developed wireless sensors based on inductive coupling that can transmit information regarding fuel centerline temperatures and rod internal pressures wirelessly from within a fuel rod to a nearby instrument thimble. After testing these sensors in lower-power university research reactors, the next step is to perform high neutron fluence testing to characterize the performance of these wireless sensors under conditions that are more representative of the intended application—in this case, light-water reactors (LWRs). The removable Be (RB) positions of the High Flux Isotope Reactor (HFIR) at Oak Ridge National Laboratory (ORNL) provide the neutron flux, experiment volume, and access to instrument leads required to achieve these sensor testing goals.

This report summarizes the design, analysis, and assembly of the Wireless Instrumented RB Experiment 2021 (WIRE-21). This is the most highly instrumented irradiation experiment ever performed in HFIR. The experiment will use seven different sensing techniques to measure temperature, pressure, neutron flux, and neutron fluence during reactor operation. In addition to WEC's wireless temperature and pressure sensors, WIRE-21 includes an array of thermocouples, self-powered neutron detectors, spatially distributed fiber optic temperature sensors, passive SiC temperature monitors, and flux wires. The design of WIRE-21 and the cabling that was installed in HFIR also provide the infrastructure to enable accelerated, economical testing of advanced sensor technologies while leveraging the extremely high neutron flux that is available in HFIR. The containment for WIRE-21 is similar to previous RB irradiation vehicles but includes a few modifications, most notably the use of integrated compression seals to pass a larger number of sensor leads through the experiment's pressure boundary. In addition to the sensor leads, inert gas lines are passed into the experiment to enable active temperature control and the ability to pneumatically actuate a bellows-driven pressure sensor. WIRE-21 is targeting component temperatures (300–350°C) and neutron fluence levels (~10^{22} n/cm^2) that would be expected in the plenum region of LWR fuels, except for the active sensing region of the wireless temperature sensor, which is targeting LWR fuel centerline temperatures (~800–1,100°C). WIRE-21 was successfully assembled, passed all nondestructive examination, and was delivered to HFIR for insertion during upcoming cycle 498 (April 2022).

1. INTRODUCTION

Nuclear reactors require instrumentation to control the fission process, ensure safe plant operation, and monitor process variables to maximize system efficiency. A wide range of reactor concepts have been demonstrated and safely operated over the last century. However, the nuclear industry has been slow to adopt the latest technological advances in instrumentation and control, particularly for in-core instrumentation. One sensing technology that could greatly benefit the nuclear industry is wireless sensors for monitoring fuel conditions during operation. Traditionally, the centerline temperatures and internal pressures of fuel rods are estimated only by using conservative calculations based on prior experiments performed in test reactors. The ability to monitor these conditions during operation could reduce unnecessary conservatism, potentially enabling higher operating powers and providing fuel performance data that could allow the use of higher enrichments and increased fuel burnup. Additionally, instrumenting lead test rods or assemblies that contain advanced fuel materials could provide valuable performance data that could be used to accelerate the licensing process for batch reloads of these fuels. Westinghouse Electric Company (WEC) is developing sensors that measure fuel centerline temperature and rod internal pressure and wirelessly transmit the information through the fuel rod's cladding [1, 2]. The ability to wirelessly transmit through the fuel rod to a nearby receiver is attractive because the wireless transmitters could be integrated into current fuel rods without sensor leads passing through the fuel rod's pressure boundary. This would alleviate concerns regarding instrument seal failures, as well as more complex handling and disposing of fuel rods with sensor leads.

Before WEC's wireless sensor technology can be reliably deployed, the sensors must be tested under representative in-core conditions to the maximum neutron fluence expected over their operational lifetime, which can take many years, depending on the specific test reactor that is used. This poses a great opportunity to leverage the removable Be (RB) positions within the High Flux Isotope Reactor (HFIR) at Oak Ridge National Laboratory (ORNL). HFIR provides one of the highest steady-state neutron fluxes in the world [3], which enables these wireless sensors to be tested at higher fluences than what could be achieved in a realistic time frame using other facilities. For example, previous WEC sensor testing in the Pennsylvania State University Breazeale Reactor and the Massachusetts Institute of Technology Reactor reached a maximum total neutron fluence of 1.1×10^{21} n/cm^2 [1, 4], more than 10 times less than the fluence that can be achieved in ~4 months of irradiation in HFIR. However, to date, instrumented experiments in HFIR's RB positions have largely focused on using the minimum instrumentation required to quantify environmental conditions during irradiation testing of nuclear fuels or structural materials. Therefore, prior to this work, the facility's cabling and the design of the irradiation vehicle could not accommodate a large number of sensing leads, particularly for more advanced sensing technologies that require low-noise triaxial (triax) cabling or fiber optics.

This report summarizes the design, analysis, assembly, and delivery of the Wireless Instrumented RB Experiment 2021 (WIRE-21) to test WEC's wireless sensor technology in HFIR to accelerate neutron fluence accumulation and move this sensing technology closer to deployment. A previous report [5] summarizes the initial experiment design, and some of the information from that report is replicated here for completeness. Two wireless sensors are being tested to measure the temperature of a reactor fuel surrogate (FS) and the displacement of a pressurized bellows during irradiation. In addition to WEC's sensors, the experiment also includes a multitude of active and passive instrumentation to measure local and distributed temperatures, as well as neutron flux, spectrum, and fluence over several HFIR cycles. This report summarizes the mechanical design for WIRE-21, the experimental test matrix, neutronic and thermal design analyses, cabling upgrades, and the experiment assembly and nondestructive examination. WEC's sensor technologies have been described previously [1, 2, 4] but are briefly mentioned in this report to describe how the experiment was designed to accommodate this specific sensor geometry. The

specific application of this sensing technology to commercial reactors is outside the scope of this work and is further subject to export control and intellectual property restrictions.

2. HFIR EXPERIMENTAL FACILITIES

2.1 HFIR CORE OVERVIEW

HFIR is a Be-reflected, pressurized, light-water–cooled and moderated flux-trap–type reactor [3]. The core comprises Al-clad involute-fuel plates, which currently use highly enriched ^{235}U fuel at a power level of 85 MWt. A typical cycle is 25 days. The reactor core, illustrated in Figure 1, comprises two concentric annular regions, each approximately 61 cm tall. WIRE-21 will be inserted into an RB position located radially just beyond the HFIR fuel at a radial distance of 27.3 cm from the center of the core. The experiment will be inserted into position 5A, shown in the lower left portion of the RB in Figure 1.

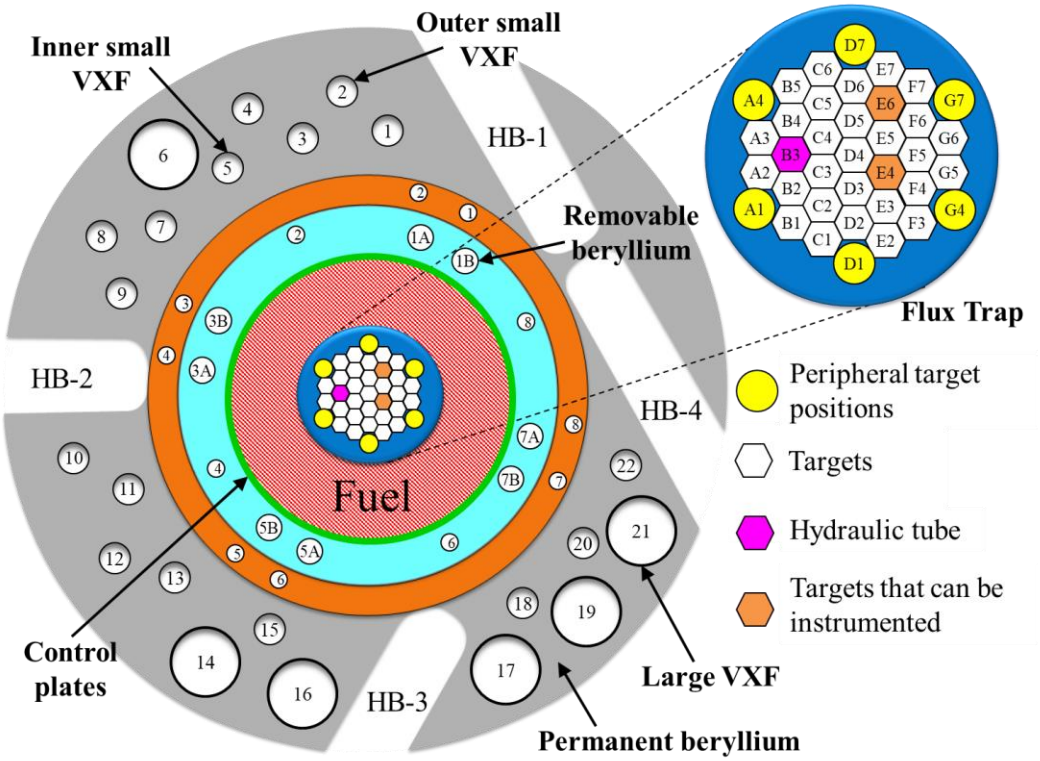

Figure 1. Schematic cross section of HFIR showing experimental positions.

2.2 MATERIALS IRRADIATION FACILITY

The Materials Irradiation Facility (MIF) is located adjacent to the HFIR pool and enables the active monitoring and control of multiple instrumented irradiation experiments simultaneously. Its primary purpose is to receive feedback from integrated experiment thermocouples and adjust the flow of various inert gases into each spatial region in an experiment. Gas flow rates are too low to cause significant convective heat removal; instead, gas flows enable online control of the gas composition inside the experiment. Nuclear heating of the internal experiment components must pass to the experiment's outer containment whose outer surface is exposed to the reactor's primary coolant. Small radial gaps within the experiment create resistances to the heat flow from the experiment's internal components. These resistances are carefully controlled by varying the composition—and thus the thermal conductivity—

through the gas gaps. Previous experiments also used the MIF to monitor the release of select fission products during instrumented irradiations of fuels [6-10]. In 2016, modifications to the facility increased the MIF's flexibility, enabling the operation of simultaneous experiments and additional instruments through software reconfigurable control modules [11]. Figure 2 shows a schematic overview of the MIF in relation to the HFIR core and the routing of sensor leads and gas lines from WIRE-21 to the MIF.

The basic building blocks of the MIF include a gas supply system, gas routing system, effluence system, and computerized software control system. The gas routing system's software is reconfigurable to meet the gas-mixture requirements of specific experiments. The gas supply system is a bank of gas bottles that can be connected to a cleanup system to remove O_2 and moisture. Removing O_2 and moisture is not necessary for this experiment because the impurity content in the as-received gas bottles is more than sufficient for the purposes of this test. He, Ne, and Ar supply gases can be used for experiments, but this experiment will only use mixtures of He and Ar. The gas routing system controls the pressure, composition, and flow rate of the gas exiting the cleanup system. The software control system uses Allen-Bradley programmable logic controllers to mix up to three different supply gases based on measured experiment temperatures, pressures, and flow rates relative to their respective set points. The gas exiting the experiment is routed to the effluence system, which includes a shielded valve box with particulate filters and holdup chambers to allow time for activated Ar and other radioactive gases to decay before being vented to HFIR's closed hot off-gas system. The control station computers display the status of the various sensor readings, set points, and radiation levels and include annunciator alarms for alerting the MIF operators and HFIR control room of any issues.

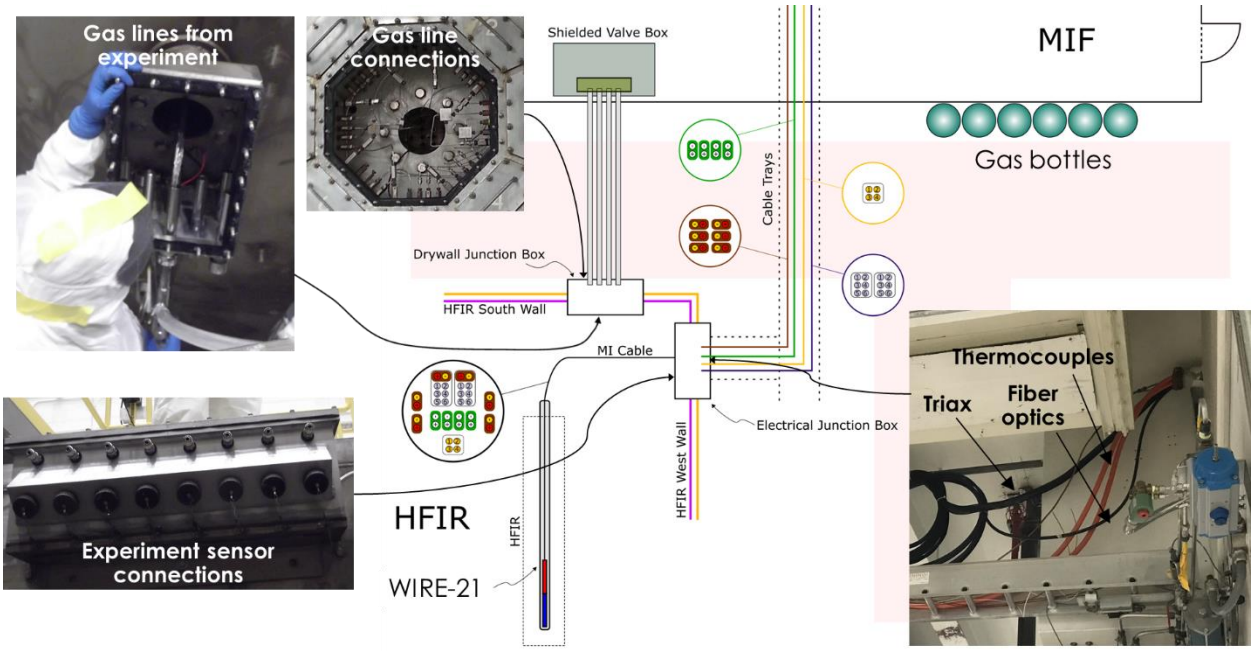

Figure 2. Schematic showing the MIF in relation to the HFIR core and the routing of sensor leads and gas lines from WIRE-21 to the MIF.

3. WIRE-21 INSTRUMENTATION

As mentioned previously, the primary goal of WIRE-21 is to test WEC's wireless temperature and pressure sensors. Additionally, the experiment contains a wide variety of passive and active instrumentation for measuring temperature and neutron flux during irradiation. Figure 3 shows a schematic detailing the location of each type of active instrumentation. Four mineral insulated cables

(MICs) transmit and receive signals from WEC's pressure and temperature sensors (two MICs per sensor), which are located above and below the HFIR midplane, respectively. One MIC traveling to each sensor contains four electrical leads for receiving signals from the reference and sensing inductors. A second MIC traveling to each wireless sensor includes two electrical leads for powering the transmit inductor and an N-type thermocouple for measuring the temperature within the FS (for the temperature sensor) and bellows (for the pressure sensor).

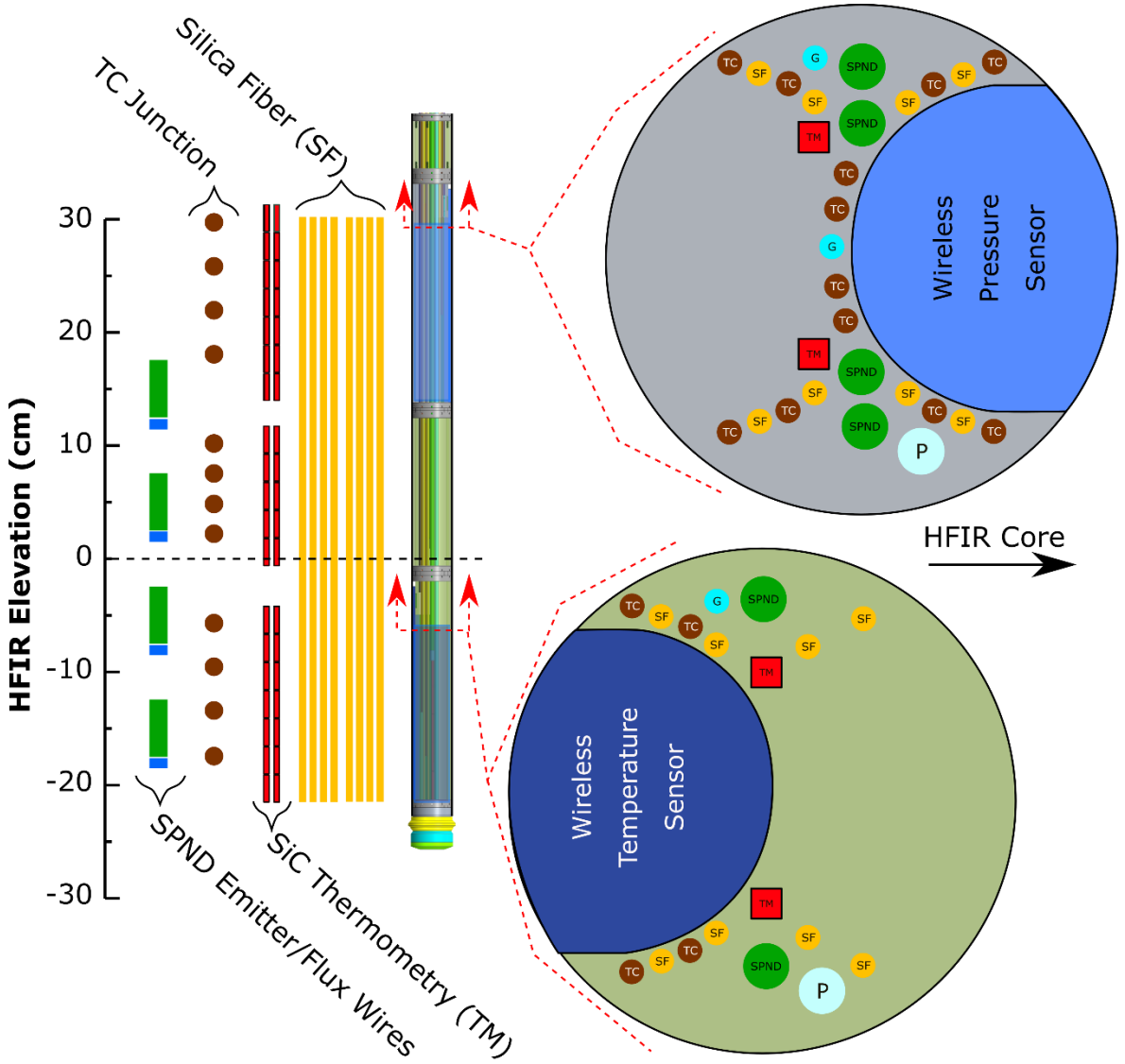

Figure 3. In-core instrumentation layout for WIRE-21 (not to scale) [12].

3.1 WEC WIRELESS SENSORS

As described previously [1, 2, 5], WEC's wireless sensors operate based on the principle of mutual inductance coupling between individual inductors. A section view of WEC's wireless sensor geometries is provided in Figure 4. A wired transmit/receive circuit energizes an inductor coil and transmits power wirelessly to a paired inductor in the passive circuit. The passive circuit also contains a reference inductor and a sensing inductor for transmitting signals back to the transmit/receive circuit. In the WEC temperature sensor, the sensing inductor's wiring is wrapped around an FS material that is designed to

operate at a higher temperature during irradiation to simulate light-water reactor (LWR) fuel temperatures. The section of Pt wire in contact with the FS acts as a resistance temperature detector (RTD) in measuring the FS temperature. Both reference and sensing inductors transmit signals wirelessly back to paired inductors in the transmit/receive circuit. The passive circuit does not require any wired connections to the transmit/receive circuit.

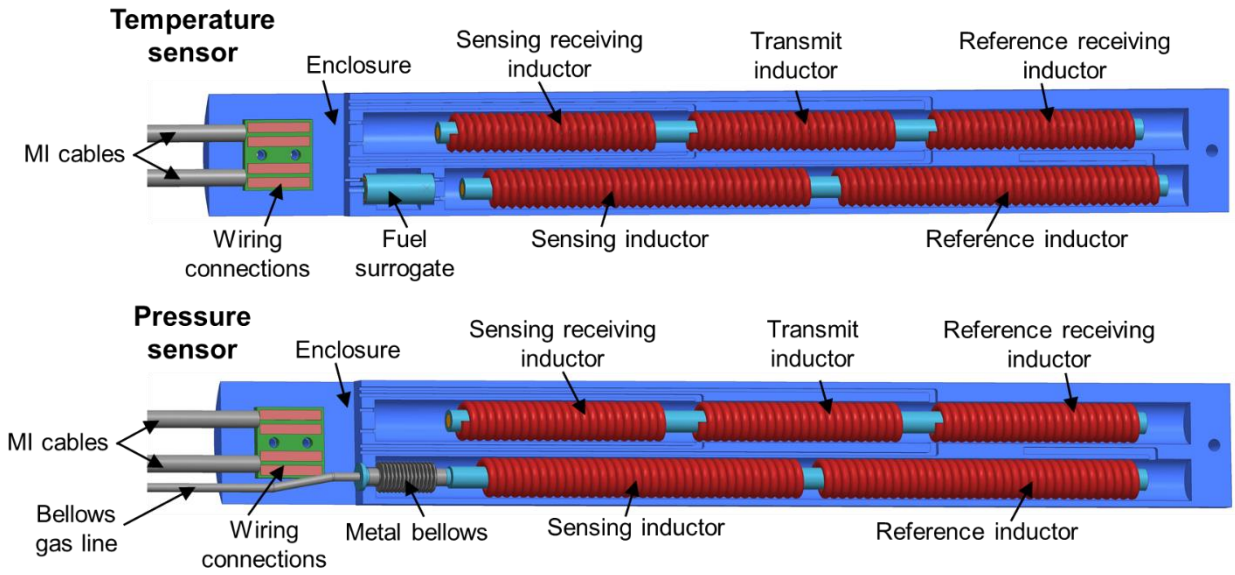

Figure 4. Section views showing WEC's wireless temperature and pressure sensors.

WEC's pressure sensor functions similarly to the wireless temperature sensor with two exceptions: (1) there is a pressurized metal bellows instead of FS material and (2) the sensing inductor core (IC) is attached to the metal bellows and free to traverse axially inside of a wire-wrapped ceramic tube. The ferritic core is coupled to the end of a metal bellows, which is pneumatically pressurized by using a gas supply system in the MIF. Increasing the static pressure supplied to the bellows causes the bellows to expand, which increases the penetration of the ferritic core inside the sensing inductor and increases the inductive coupling from the sensing inductor to its paired inductor in the transmit/receive circuit.

3.2 THERMOCOUPLES AND GAS LINES

In addition to the two thermocouples that terminate inside WEC's sensor enclosures, 12 stainless-steel–sheathed (1.6 mm or 1/16 in. diameter), MgO-insulated, N-type thermocouples (labeled TC in Figure 3) will measure local temperatures in various regions of the experiment and will provide feedback to the MIF control system. As mentioned previously, temperature control is accomplished by adjusting the composition of gas gaps within the experiment. For this, 1.6 mm (1/16 in.) diameter gas lines (G1 and G2) are routed below the upper and lower holders that contain the pressure and temperature sensors, respectively. A larger 3.2 mm (1/8 in.) diameter He purge line (P1) is also routed to the bottom of the experiment to allow the experiment to be rapidly flooded with He if unexpected high temperatures are measured. A 3.2 mm (1/8 in.) diameter effluent gas line (not shown) is located at the top of the experiment's containment and transfers the supplied gases from the experiment to the MIF's effluence system and ultimately to HFIR's hot off-gas system. A 1.6 mm (1/16 in.) diameter high-pressure gas line (HP1) provides an adjustable, steady-state internal pressure within the metal bellows that is attached to WEC's pressure sensor.

3.3 FIBER OPTIC TEMPERATURE SENSORS

The included thermocouples will provide accurate measurements of temperature at up to four discrete locations within each holder and provide feedback to the MIF temperature control system. Additionally, eight spatially distributed fused silica fiber optic temperature sensors (denoted as *silica fibers [SF]*) will provide a more detailed temperature mapping along the experiment length. Optical fibers are an attractive option for temperature-sensing applications because they are small and can provide spatially distributed (millimeter-scale) measurements over tens of meters along one optical fiber. The fibers that will be tested are summarized in Table 1. All sensing fibers are single mode operating near 1,550 nm with varying core/cladding dopants, some with fiber Bragg gratings (FBGs) [13] and some with a hollow core. The FBGs were inscribed with either an ultraviolet (UV) continuous wave laser or a pulsed femtosecond laser to provide strong reflections for analyzing the backscattered light signal. Whether the reflections originate from intentional Bragg gratings or from Rayleigh backscatter from random density fluctuations in the amorphous structure, distributed temperature measurements are made by analyzing these reflected signals using optical frequency domain reflectometry [14, 15]. Although the fiber optic sensors may suffer from radiation-induced attenuation after prolonged neutron exposure [16, 17], they should provide accurate temperature distributions during the early phase of the irradiation to inform the temperature gradients within the sensor enclosure. All sensing fibers were fusion spliced to at least 3.6 m of SMF1250SC(9/125)P (pure silica core, F-doped silica cladding) lead fiber before transitioning to SMF-28e+ above the top of the reactor pressure vessel. SF1 through SF6 were terminated with a coreless termination fiber to prevent significant back reflections from affecting sensing measurements near the end of the sensing fiber. SF7 and SF8—the hollow core fibers—were terminated with ordinary single mode fiber so that the Rayleigh backscatter amplitudes before and after the hollow core section could be compared. All fibers were sheathed inside 316 stainless-steel tubes with a 1.6 mm (1/16 in.) outer diameter (OD) and 0.25 mm (0.010 in.) wall thickness.

Table 1. Summary of fiber optic sensors included in WIRE-21.

Fiber	Description	Vendor	Part number	Length	Gratings
SF1	Pure SiO_2 core, F-doped SiO_2 cladding	Fibercore	SMF1250SC(9/125)P	1.22 m + ~10 cm coreless termination	N/A
SF2	Ge-doped SiO_2 core, pure SiO_2 cladding	Corning	SMF-28e+		
SF3	F-doped SiO_2 core and cladding with femtosecond gratings	Fujikura, gratings inscribed by FemtoFiberTec	N/A (custom fiber) + 9 femtosecond gratings		~1% reflectivity, ~65 mm spacing
SF4			N/A (custom fiber) + 6 femtosecond gratings		
SF5	Pure SiO_2 core, F-doped SiO_2 cladding with femtosecond gratings	Fibercore, gratings inscribed by FemtoFiberTec	SMF1250SC(9/125)P + 28 femtosecond gratings		~3% reflectivity, ~10 mm spacing
SF6	Low bend loss SiO_2 fiber (proprietary dopants) with UV gratings	FBGS	AGF-A3A4-000		<0.1% reflectivity, 10.5 mm spacing over entire length
SF7	Hollow core photonic crystal fiber	NKT Photonics	HC-1550	1.22 m + ~15 cm SMF1250SC-(9/125)P	N/A
SF8					

3.4 SELF-POWERED NEUTRON DETECTORS

Four self-powered neutron detectors (SPNDs) were included in WIRE-21 to measure the real-time neutron flux distribution within the experiment. SPNDs comprise two concentric electrodes: a conductive outer sheath (collector) and a neutron-sensitive wire (emitter) that emits a beta particle (electron) upon neutron capture [18]. An insulating material separates the collector and emitter, and an electric field caused by the accumulated space-charge develops that resists electron flow. When deployed in a reactor, neutron absorption in the emitter generates sufficiently high-energy electrons to overcome the electric field and stopping power of the insulating material, resulting in a small electrical current (A_1) between the emitter and collector. WIRE-21 uses V emitters and Inconel 600 for the collector outer sheath and the lead wire that is joined to the emitter. A second Inconel 600 electrical lead was included inside the sheath without an attached emitter to compensate for the current (A_2) generated from gamma interactions along the length of the SPND. A differential measurement of the currents from the two leads results in a DC current proportional to the neutron flux alone at the location of the emitter wire. The SPNDs have an ~83 mm (3.25 in.) long larger diameter region in the in-core region that surrounds the emitter that transitions to 3.18 mm (⅛ in.) OD MIC above the core. The relevant parameters for the SPNDs are summarized in Table 2.

.

Table 2. SPND parameters.

Parameter	Value
Sheath/collector material	Inconel 600
Insulation material	MgO
Emitter material	V
Emitter and compensation wire material	Inconel 600
In-core sheath dimensions	3.96 mm OD × 0.38 mm wall × 83 mm long (0.156 in. OD × 0.015 in. wall × 3.25 in. long)
Emitter wire dimensions	0.51 mm diameter × 50.8 mm long (0.020 in. diameter × 2 in. long)
Emitter and compensation wire diameter	0.51 mm (0.020 in.)
MIC sheath and wire materials	Inconel 600
MIC sheath dimensions	3.18 mm OD × 0.58 mm wall (0.125 in. OD × 0.023 in. wall)
MIC wire diameter	0.51 mm (0.020 in.)
MIC insulation material	MgO (>70% dense)

3.5 PASSIVE SIC TEMPERATURE MONITORS

SiC materials accumulate radiation-induced point defects that reach an equilibrium within a temperature range of ~200 to 1,000°C, and the equilibrium defect concentration is highly temperature dependent within this range [19]. Furthermore, those point defects measurably affect many macroscopic properties. This can be exploited by monitoring macroscopic properties post-irradiation during controlled thermal annealing. In this way, SiC specimens can be inserted into the irradiation vehicle, and the irradiation temperature can be determined based on the post-irradiation annealing behavior. WIRE-21 has 38 passive SiC temperature monitors (TMs) located throughout the experiment, particularly near the thermocouples and fiber optic sensors. These sensors will enable the in situ measurements from fiber optics and thermocouples to be directly compared with the passive measurements that will be obtained post-irradiation. The TMs are 25.4 mm long with a 2 mm square cross section. They will be evaluated post-irradiation using continuous dilatometry (i.e., recovery of radiation-induced dimensional changes) [20].

3.6 PASSIVE NEUTRON FLUENCE MONITORS

The total neutron fluence will be passively monitored by measuring the post-irradiation activity of several wires, called *flux wires*, that are sealed inside small V capsules. The average neutron flux energy spectrum can then be deconvolved by using a spectrum unfolding code. Four capsules will be included, and one capsule is positioned directly beneath each of the four SPNDs. This will enable the comparison and calibration of the in situ neutron flux measurements from the SPNDs. The wire materials include Fe, Ti, Nb, Cu, and Al with 0.1% Co.

4. WIRE-21 DESIGN

4.1 IN-VESSEL EXPERIMENT REGION

Figure 5 provides a general overview of the experiment containment and internal components. The in-core region of WIRE-21 comprises four axial subsections: the lower holder, lower spacer, upper holder, and upper spacer (from bottom to top). Each holder and spacer is separated by a pair of centering thimbles

fastened to each subsection. The red dashed lines and associated text in Figure 5 indicate the elevations of the HFIR midplane and the top of the HFIR reflector. WEC's wireless pressure sensor is placed inside the upper holder with the top of the pressure sensor enclosure coplanar with the top of HFIR's fuel element. The lower holder contains WEC's wireless temperature sensor with the top of the sensor located 5 cm below the HFIR midplane. The upper spacer serves as a guide for the sensor leads and helps dissipate nuclear heating in the leads to prevent them from overheating. The lower spacer serves a similar function but also contains four thermocouple junctions (red leads), two SPNDs (blue leads), two flux wire dosimetry capsules (green cylinders below SPNDs), four optical fibers (yellow leads), and 14 SiC TMs (stacked red paralepidids).

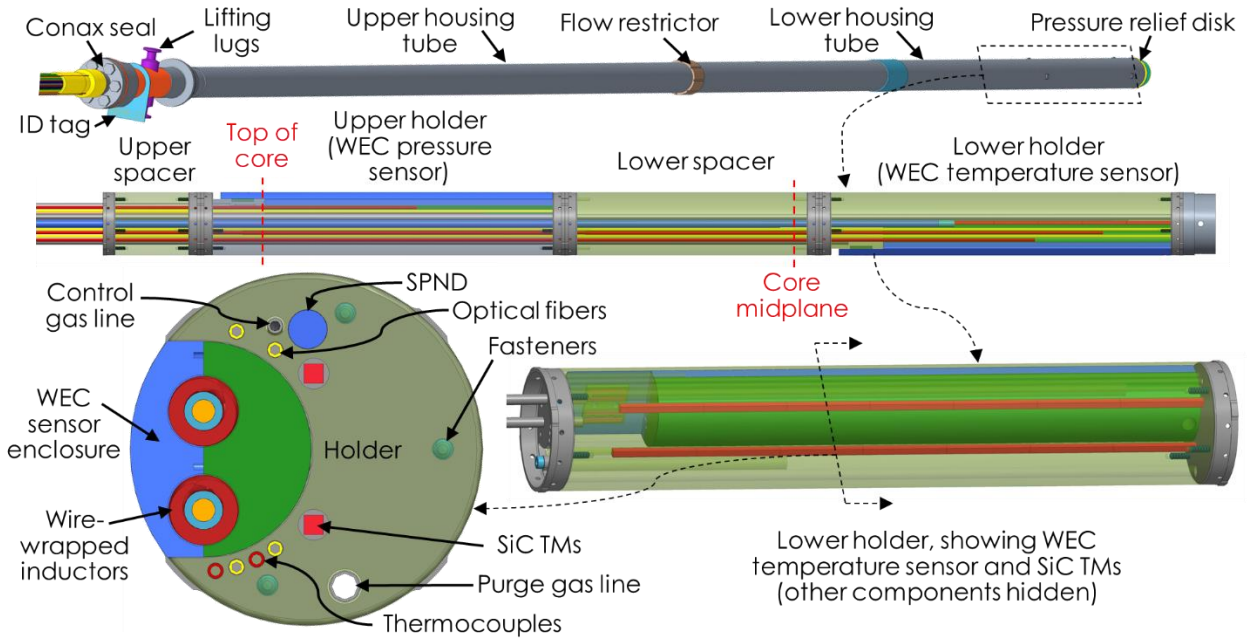

Figure 5. In-vessel region of WIRE-21 with detail views showing the temperature and pressure sensor holders.

Cross-sectional views of the upper holder, lower spacer, and lower holder are shown in Figure 6, which indicates where the various types of active and passive instrumentation are located. Semitransparent symbols represent instrumentation that passes through the subsection but terminate in a lower region. The experiment will be oriented so that the radial center of the HFIR core is located on the right in Figure 6. The light green regions in the figure represent the graphite holder or spacer, and the light gray region represents the WEC pressure or temperature sensor. Flux wire dosimetry capsules are located coaxially with and directly below the distal end of each SPND.

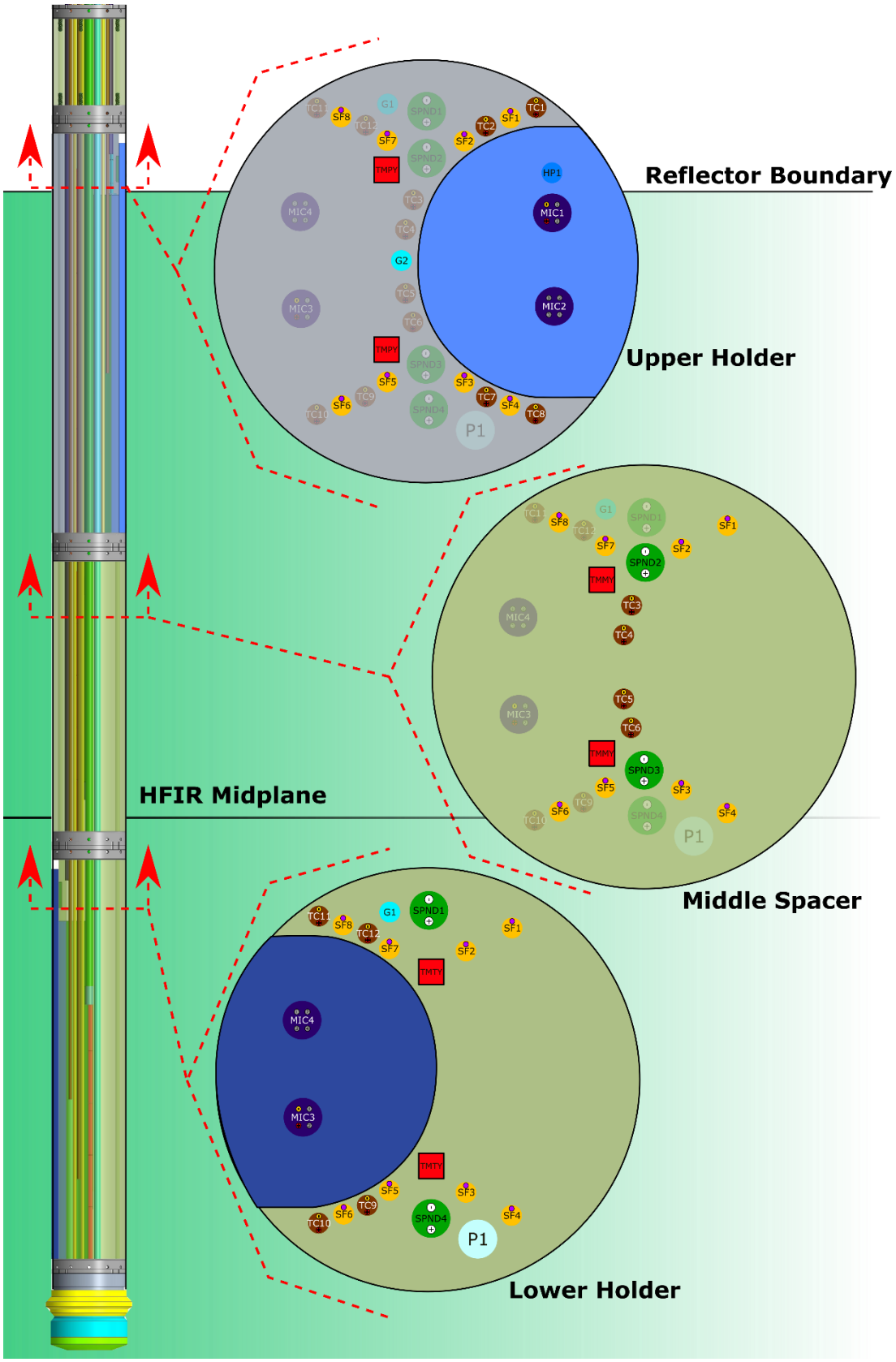

Figure 6. Instrumentation and gas line layout for three primary experiment locations.

Most of the experiment will be contained within the lower and upper housing tubes, which are both welded to a weld coupler located above the in-core region. The end of the lower housing tube is welded to an adapter and a rupture disk that will burst if the experiment is unintentionally over-pressurized. Centering tabs on the lower housing tube keep the experiment centered within the channel of HFIR's RB position, and a welded flow restrictor includes small, machined channels that introduce a sufficiently large flow resistance to prevent the experiment from redirecting too much coolant flow away from HFIR's fuel. The top of the upper housing tube is welded to an upper bulkhead located just below the lifting lugs with a machined o-ring groove that allows the experiment to seal against the top lid of HFIR's pressure vessel. Above this seal, lifting lugs allow the experiment to be raised and lowered into the HFIR pool, and a welded tag with an engraved identifier helps operators identify the experiment. Above these components, a compression seal (or Conax seal) for the sensor leads is welded to the experiment.

The sensor leads pass through a shield plug (not shown), which contains spiral channels that prevent radiation from streaming up through the experiment's housing during post-irradiation handling. The leads continue upward until they reach the compression seal. The compression seal used in this experiment is a 316 stainless-steel MHM6 seal from Conax Technologies with a weld neck and a "B" cap, which includes an integrated pipe thread. This seal includes an internal grafoil sealant, which is compressed by six hex head screws as the seal's cap presses against an internal stainless-steel follower. When properly torqued, the follower compresses the sealant around the leads, filling the void space and creating a gas-tight seal. A custom gasket is placed between the body and the top cap of the compression seal so that HFIR pool water does not collect inside the cap. The cap is welded to a hose adapter, which allows a polyurethane hose to be secured via hose clamps to keep the leads dry as they pass to the top of the HFIR pool. To further reduce the probability of internal gas leakage, the top cap of the compression seal was filled with epoxy.

4.2 HFIR POOL REGION

The WIRE-21 containment extends from the core up to just above the quick opening hatch where the experiment is sealed from the reactor's primary coolant (Figure 7a). The leads that pass beyond the compression seal are guided through the reactor pool inside a 31.75 mm (1.25 in.) inner diameter polyurethane flexible hose (Figure 7b). A Y-adaptor assembly is used to split the hose to provide a path for gas lines to pass through the in-pool junction box to the dry wall junction box, which includes permanent gas lines that pass to and from the MIF (Figure 2). All other experiment leads are routed out of the other end of the Y-adaptor in a second polyurethane hose to an experiment-specific junction box, hereafter referred to as the *experiment junction box*. The Y-adaptor contains two hose fittings for securing the hose with hose clamps and one compression-style fitting that is attached directly to the in-pool junction box.

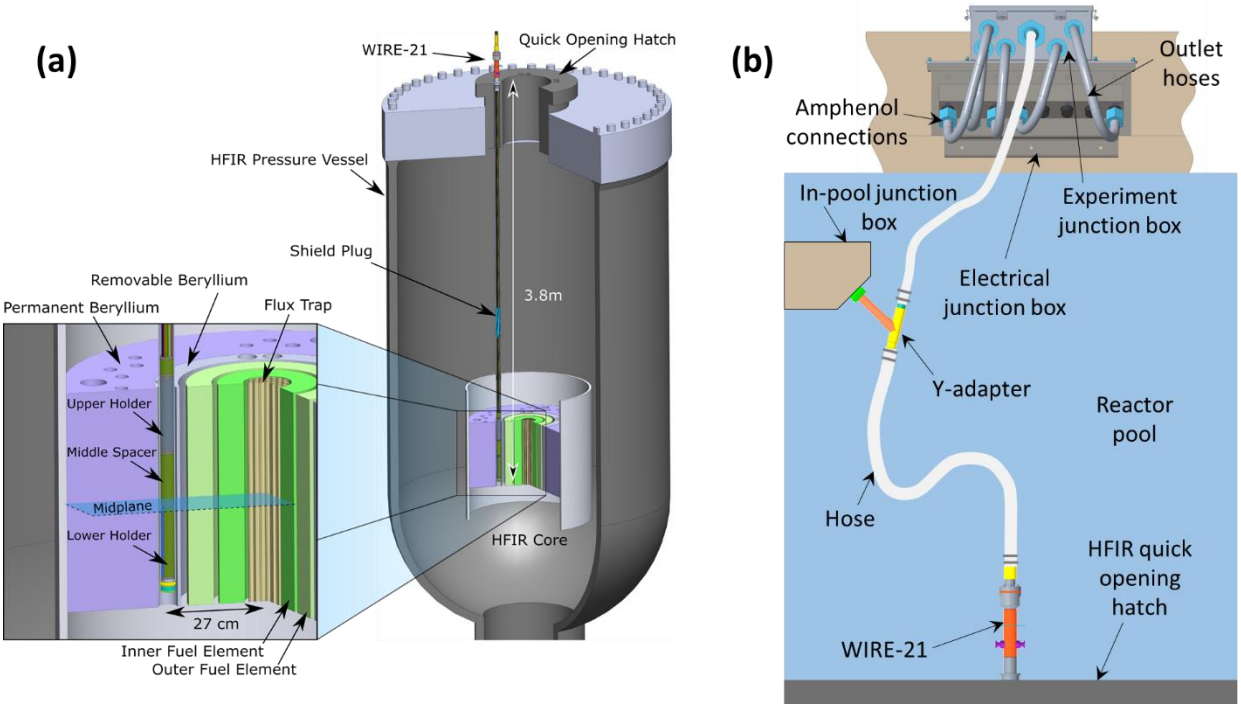

Figure 7. (a) Model showing WIRE-21 inside an RB position passing up through HFIR's quick opening hatch [12] and (b) a schematic (not to scale) showing the experiment leads passing up through the reactor pool to the various junction boxes.

The hose exiting the Y-adaptor passes up to the top of the HFIR pool where it is attached to the experiment junction box with a hose clamp and barbed tube fitting. This barbed tube fitting is attached via a national pipe thread to a tank fitting installed on the wall of the experiment junction box. Each of the various groups of sensors (i.e., thermocouples, triax, and fiber optics) transition to flexible leads inside the experiment junction box, which is described in more detail in Section 4.3. The flexible leads are then separated into separate, smaller hoses, labeled *outlet hoses* in Figure 7b, that terminate with Amphenol plugs. Those Amphenol plugs connect to mating receptacles inside the electrical junction box. More details regarding the design of the experiment junction box and the routing of sensor leads from the experiment junction box to HFIR's electrical junction box are provided in Section 4.3.

4.3 POOLSIDE ELECTRICAL CONNECTIONS

The sensor leads that pass from the Y-adaptor to the experiment junction box include the MICs for WEC's wireless sensors and the SPNDs, the stainless-steel–sheathed Type N thermocouples, and the fiber optic temperature sensors. Figure 8 shows a schematic of the cabling that will enter the experiment junction box, as well as the individual outlet hoses that will terminate with Amphenol plugs that mate with corresponding Amphenol receptacles in the HFIR electrical junction box. The lower layer includes a custom electronics board that includes ORNL-developed connectors for terminating the MICs, as well as analog circuitry that amplifies the output signal from the SPNDs and WEC sensors. The board also converts the SPND signals to voltages and compensates for contributions from gamma interactions by subtracting the readings from the gamma compensation wires. Figure 9 shows more details of the electronics board. Flexible cables are used to carry signals from the output of the board to the Amphenol plugs. Similarly, the stainless-steel–sheathed thermocouples transition to flexible thermocouple extension wires in the top layer of the experiment junction box. The fiber optic sensors are coupled to jacketed patch cables via angled polish (LC/APC) connectors. One Amphenol plug is used for all 14 thermocouples, including the two thermocouples located inside WEC's sensor enclosures. Similarly, all

eight fiber optic sensors are terminated via one single Amphenol plug. The MICs for the SPNDs and wireless sensors are split across three triax Amphenol plugs. One triax pin will be used to provide a direct current power supply to preamplify the SPND and wireless sensor signals. Linear regulators with large decoupling capacitors at their inputs will be used to step down the voltage from ±24 V, as generated at the MIF, to ±15 V at the input of the preamplifier circuitry.

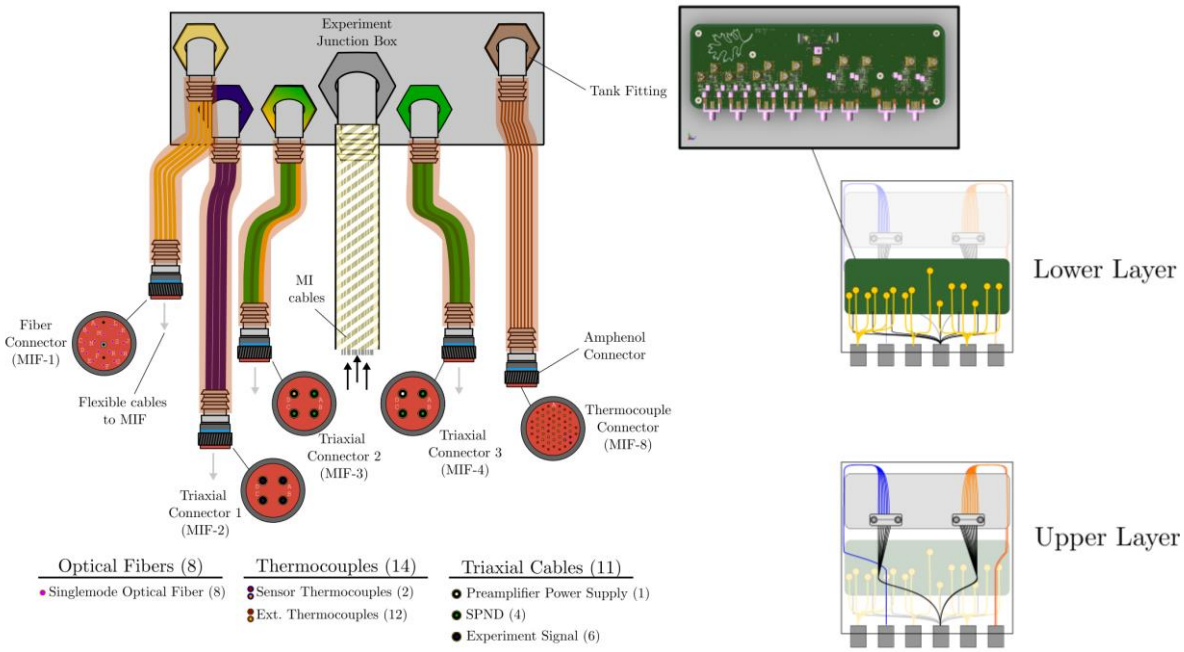

Figure 8. Cabling schematic for the experiment junction box (left) and schematic showing the internal connections within the experiment junction box (right).

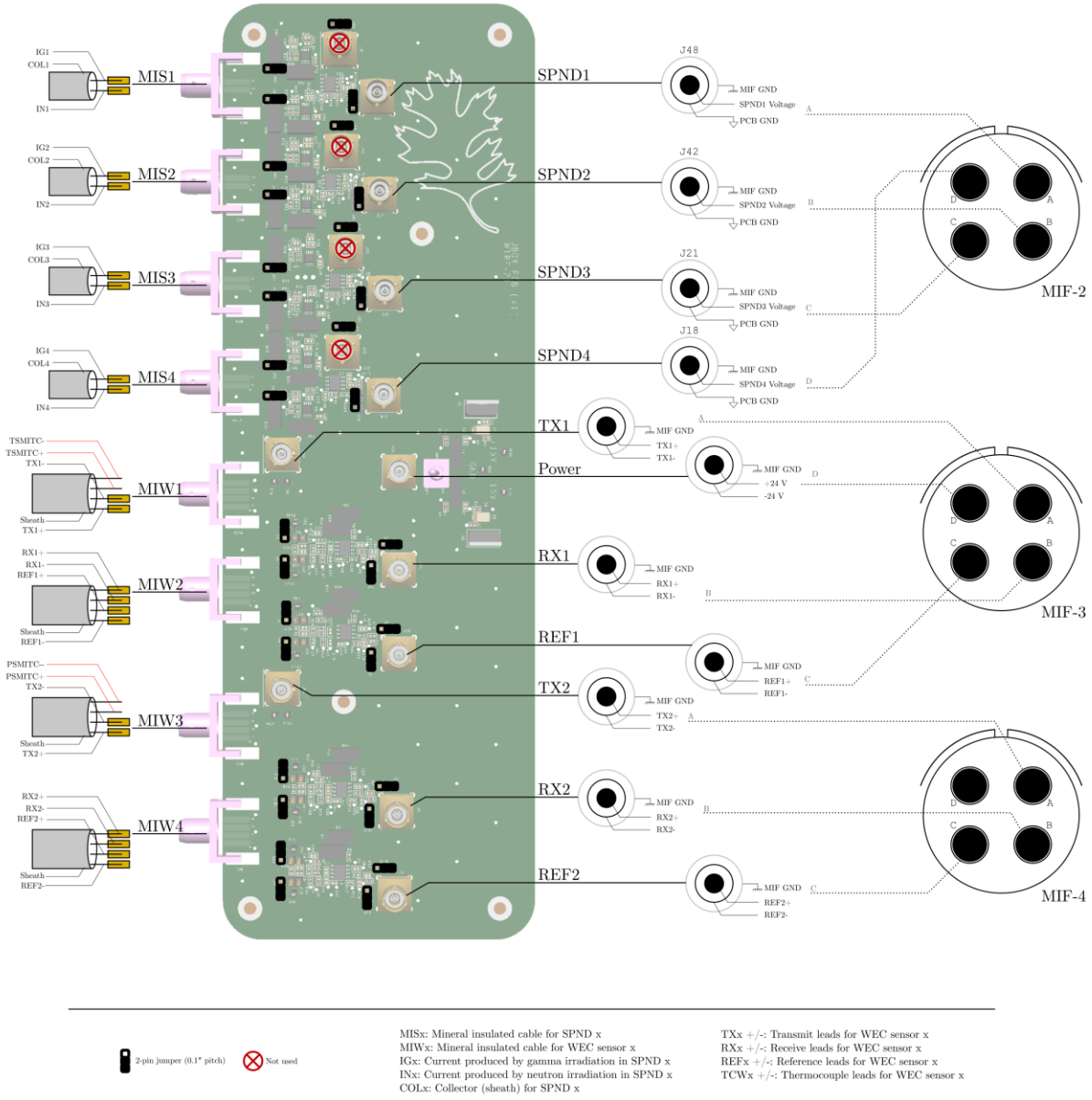

Figure 9. Detailed electrical diagram for the board within the experiment junction box.

The drive signal (TX) for the wireless sensors must be transmitted from equipment in the MIF to the transmitting inductors shown in Figure 4. Because the signal must couple wirelessly to and from the sensing and reference inductors, the two inductively coupled output signals—the reference signal (REF) and sensing signal (RX)—have relatively small current outputs. Therefore, special provisions were made to maintain signal integrity over these long lengths. MICs were run with the outer conductor connected to earth ground in the MIF to provide shielding for the signals carried on the internal conductors. Additionally, RX and REF signal preamplification is performed on the board inside the experiment junction box before transmitting the signal over long cable lengths to the data acquisition systems in the MIF. These preamplifiers use an instrumentation amplifier to reject the common-mode noise present on the RX and REF signals.

As the SPNDs pass through the approximately 4 m long experiment containment, their sheaths will be grounded to the experiment housing, which could inject noise into the measurements. To overcome this challenge, the board enables a data acquisition system to measure a voltage across a series resistance within the DC current loops from each of the SPND emitters to the common collector [21]. This voltage can then be amplified by a preamplifier, and a differential voltage measurement can be performed between the two signals by using an instrumentation amplifier. Although this approach requires additional components to generate an analog differential signal between the emitter and compensation wires, it does not require that the two signals have the same ground reference, and it dramatically reduces the common mode noise present in each of the signals due to the common collector. Alternatively, the SPND signals can bypass the board, and the currents from the SPNDs can be directly recorded by using traditional picoammeters. The SPND signals will be passed along the same type of triax cables as WEC's sensors to mitigate noise injection. The middle conductor of the triax cables will carry the signal ground, and the center conductor will carry the signal. In this configuration, the earth-grounded outer conductor will shield the internal conductors as the signal is carried from the preamplifier in the experiment junction box to the MIF.

5. MODELING

5.1 NEUTRONICS AND DEPLETION MODELING

Neutronics analyses provide critical information for in-core irradiation experiments, including material heat generation rates, displacement damage, transmutation, neutron flux energy spectra, and potential effects to reactor operations, such as reactivity worth and neutron flux tilt. This is especially important for HFIR experiments because materials are exposed to an extremely high thermal neutron flux on the order of 10^{15} n/cm^2/s and gamma heating on the order of 10 W/g [22]. For WIRE-21, the primary goal of the neutronics analysis is to determine the spatial and time dependence of neutron, photon, and decay heating in the experiment materials. Neutron activation must also be estimated to provide input to post-irradiation shipping and handling of the experiment. Neutronics modeling results also provide local neutron flux energy spectra that are used in neutron spectrum unfolding codes when analyzing the activation flux wires included in the experiment.

Total nuclear heat generation rates with contributions from prompt neutron, prompt gamma, delayed fission product gamma, and local activation heating were modeled by using the HFIRCON [23] software code. HFIRCON provides coupling and data handling between radiation transport (MCNP-TN), depletion (ORIGEN-S), and variance reduction codes (ADVANTG) to calculate heat generation rates and neutron flux distributions throughout each HFIR cycle. A simplified 3D geometry of WIRE-21, located in the RB position of HFIR, was modeled for 10 time steps over a typical HFIR cycle that could last up to 26 days. All experiment components were divided into 1 cm axial slices to capture axial spatial variations in the heat generation rates. The model also accounts for the fact that WEC's pressure sensor is located closer to the radial center of HFIR's core (core position), whereas WEC's temperature sensor is located further from the core (reflector position). Control plate movement over the course of a typical HFIR cycle was also included in this model by using historical positions of the control plates that were required to achieve criticality. The total heat generation rates for material m were fit to a Gaussian function by using linear-least squares regression:

$$\dot{Q}_m(z) = A_{m,d} \times exp\left(-\left[\frac{z-z_{0_d}}{\sigma_d}\right]^2\right), \quad (1)$$

where $\dot{Q}_m$ is the material-specific heat generation rate at displacement z (in cm) from the midplane, $A_{m,d}$ is the material-specific peak heat generation rate for a specific cycle day d, z_{0_d} is the axial location of the peak heat generation rate for a specific cycle day, and σ_d is a measure of the axial distribution of the power profile. Appendix A summarizes the fitting parameters for all materials and cycle times that were used to determine the heat generation rates used in the finite element thermal analyses. Peak heat generation rates in all materials were found to drift below the midplane over the course of one cycle because of control plate withdrawal, as shown in Figure 10. More specific details of the neutronics models, methods, geometry, and materials are provided in a previous report [5].

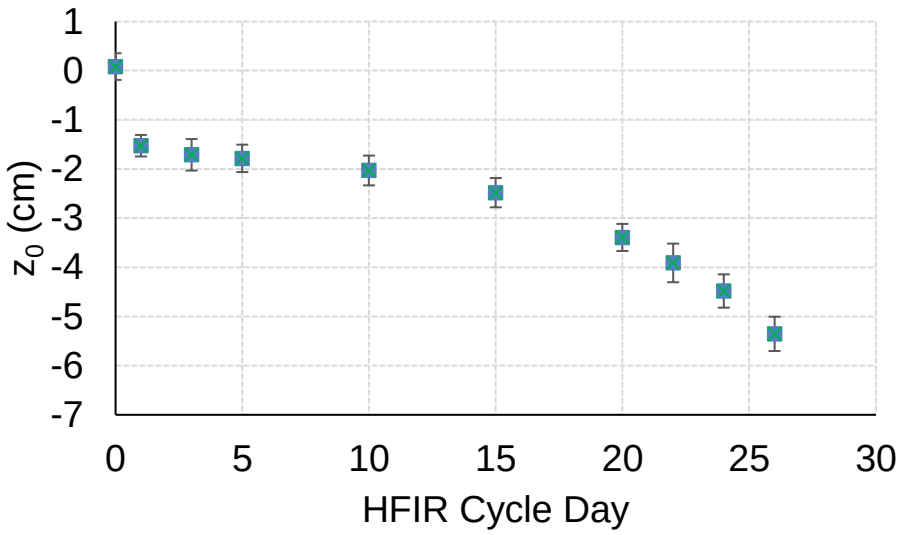

Figure 10. Location of the peak heat generation rates (z_0) relative to the HFIR core midplane vs. time relative to the start of a HFIR cycle.

5.2 FINITE ELEMENT THERMAL MODELING

Although WIRE-21 contains many types of passive and active instrumentation, in-pile testing of the prototype sensors developed by WEC is the primary purpose for conducting this experiment. Therefore, achieving optimal neutron flux and temperature conditions for these two sensors was the principal design goal of WIRE-21. Sensors within the experiment assembly were modeled by using the ANSYS 19.2 finite element analysis code for a range of parameterized input conditions, including the geometric dimensions, materials, axial location within the RB position, and several other variables. Table 3 summarizes the important parameters used in the simulations.

Table 3. Parameters used in the finite element analysis modeling.

Parameter	Value
Coolant inlet/outlet temperature	49.0–53.4 °C
Coolant mass flow rate	22.6 gpm
Surface heat transfer coefficient	30.2–31.2 kW/m^2
Capsule surface temperature	50.2–70.5°C
Internal gas composition	0–30 %Ar, balance He
Day of HFIR cycle	0–26
Housing inner diameter	37.1 mm
Upper spacer OD	35.82 mm
Upper holder OD	36.62 mm
Lower spacer OD	36.98 mm
Lower holder OD	37.00 mm

The inductors were modeled with an Fe core, surrounded by thin-walled alumina tubing, and tightly wrapped with Ni-clad Cu wire. All ICs were modeled as pure Fe for the cases summarized here, although the final sensor uses a Si–Fe alloy. More details regarding the thermal modeling approach are described in another work [5]. The target temperatures for this experiment include:

- a nominal temperature of 300–350°C for the ICs;
- a maximum IC temperature of 500°C, except during brief periods of operation during which there may be interest in temporarily exceeding the Curie point of the ICs;
- a nominal temperature of 800–1,100°C for the FS; and
- the ability to change temperature via HFIR control plate movement and/or gas composition changes.

Figure 11 shows contour plots of the expected temperature distributions in the temperature and pressure sensors, as well as the fiber optic sensors located in the surrounding graphite holders, at the end of a HFIR cycle with a 15% Ar (He balance) gas composition. The pressure sensor shows relatively low temperatures near the bellows (~200°C) that increase to >350°C near the bottom ICs. The temperature sensor shows more uniform temperatures in the range of 400°C in the ICs with a peak temperature in the FS of ~1,200°C. The fiber optic sensors show an axial variation in temperature that varies from 165°C at the top of the experiment to as high as 479°C in the region between the lower holder and lower spacer.

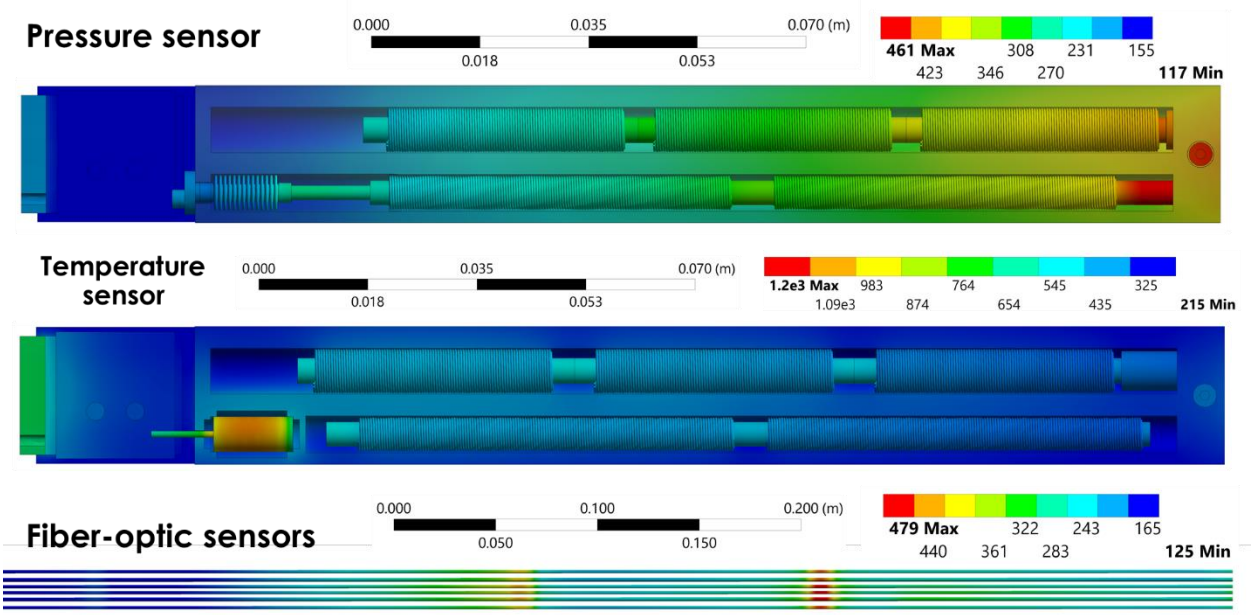

Figure 11. Calculated temperature distributions (in degrees Celsius) in WEC's pressure and temperature sensors and the fiber optic sensors at the end of a HFIR cycle with a 15% Ar (He balance) gas composition.

Figure 12 shows the numbering convention for each inductor in the pressure and temperature sensors, as well as the variation in the temperatures of the ICs, TCs, FS, and FS TC during day 1 and day 25 of a HFIR cycle. Error bars correspond to the maximum and minimum temperatures of each component with the average temperature indicated by colored markers. Results are shown with 100% He gas gaps, but Ar can be added to increase temperatures, as needed. Detailed summaries of experimental temperatures in all components as a function of time and Ar concentration are available and summarized in Appendix B. The pressure sensor temperatures generally decrease with increasing time in a HFIR cycle as the peak heat generation rates move to lower elevations, which results in decreased heating within the pressure sensor. This phenomenon has a lesser effect on the temperature sensor, which is located closer to the core midplane. However, the fission density in the HFIR fuel also moves radially outward throughout the cycle as the control plates are withdrawn. This causes heating rates to increase in the temperature sensor, which causes component temperatures to increase with increasing time.

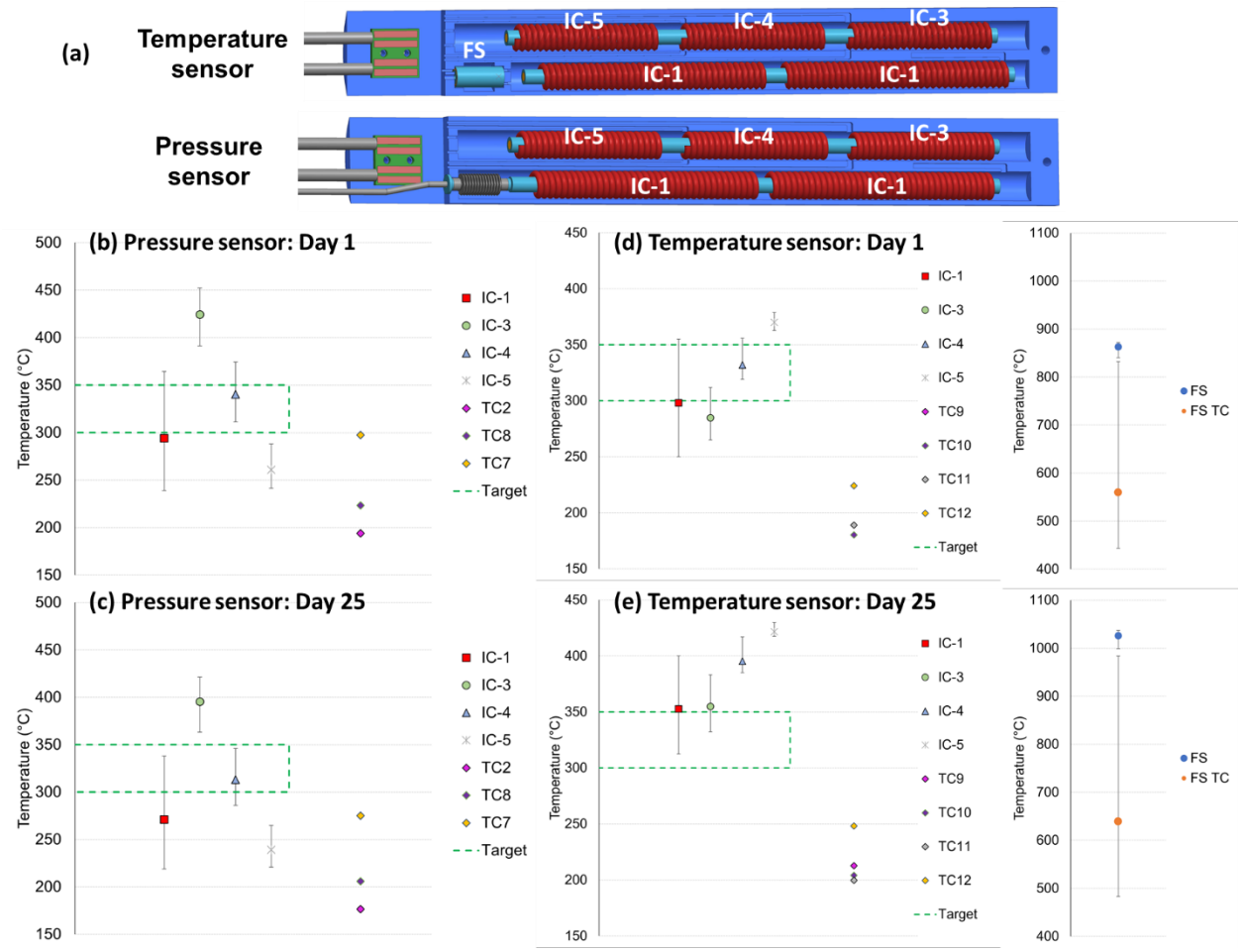

Figure 12. (a) Labeling of ICs in the temperature and pressure sensors, (b)–(c) temperatures in the pressure sensor's ICs and TCs during days 1 and 25 of a HFIR cycle, and (d)–(e) temperatures in the temperature sensor's ICs and TCs and in the FS and FS TC during days 1 and 25 of a HFIR cycle.

Results indicate that IC temperatures can generally be maintained within the desired 300–350°C range, except for IC-3 in the pressure sensor for all times and all ICs in the temperature sensor at the end of a cycle. The FC TC shows a wide variation due to the volume chosen for this component, but the TC junction will be located at the end of the TC probe, which will measure a temperature close to the maximum temperature shown in Figure 12d and Figure 12e. These temperatures are within the desired range of 800 to 1,100°C.

6. ASSEMBLY, TESTING, AND DELIVERY TO HFIR

6.1 EXPERIMENT ASSEMBLY

WEC assembled its temperature and pressure sensors and shipped them to ORNL with the long MI cables and static pressure line coiled inside a large crate. The sensors were examined for damage caused during shipping and were found to have sustained no damage, except for small bends in the MI cables, which were straightened at ORNL. Figure 13 shows photographs of the assembled sensors with and without the top covers installed. The internal photograph of the temperature sensor was taken before installing the FS and its TC, so those components are shown schematically for reference.

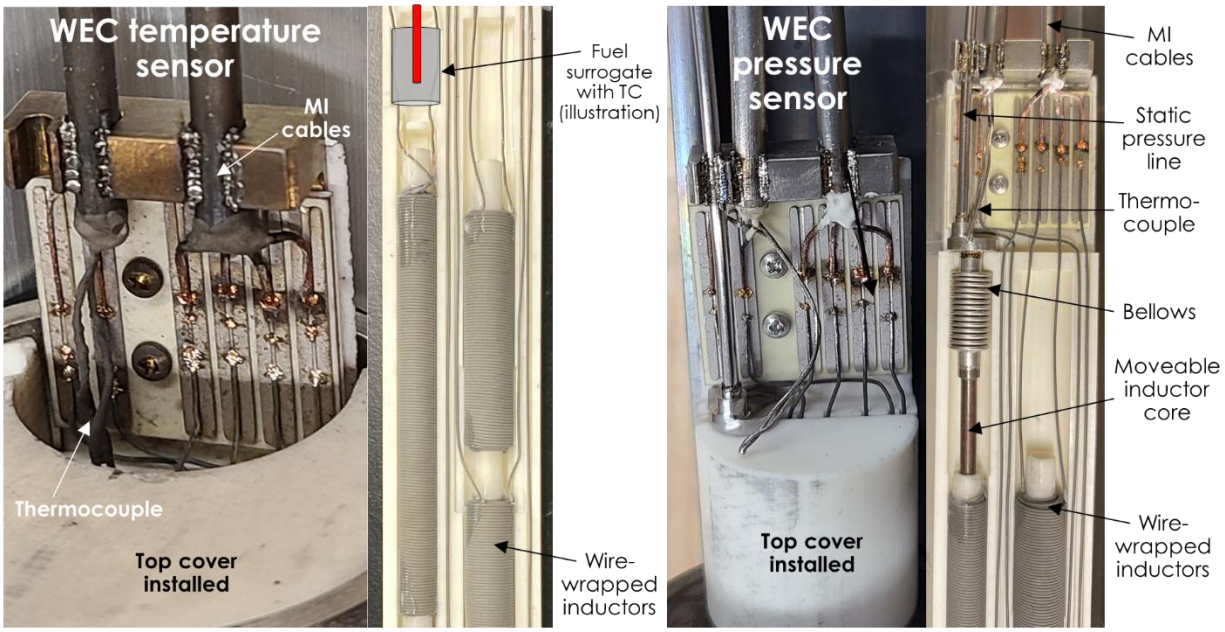

Figure 13. WEC's temperature (left) and pressure (right) sensor enclosures with and without the top cover installed. The photograph of the temperature sensor was taken before installing the FS and its enclosed thermocouple, so these parts are illustrated for reference.

The SPNDs and TCs were procured from Idaho Labs Corporation. Figure 14 shows photographs of the region near the emitter of one SPND, as well as the passive SiC TMs and the flux wire dosimetry capsules. The SPNDs have a larger diameter near the emitter region, which improved fabricability, but are reduced down to a standard size 3.18 mm (⅛ in.) diameter MI cable to be compatible with the holes in the compression fitting at the top of the experiment. The flux wire dosimetry capsules were bonded inside quartz ampules by using a high-temperature adhesive to make them easier to handle post-irradiation.

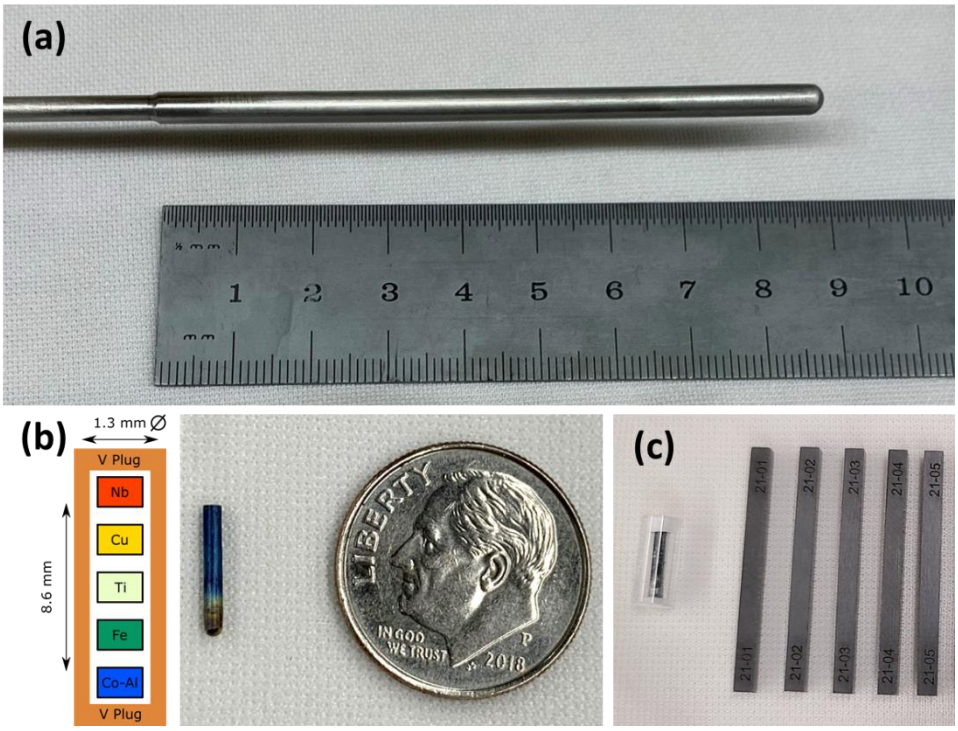

Figure 14. (a) The region near the emitter of a SPND, (b) schematic and photograph of a flux wire dosimetry capsule, and (c) dosimetry capsule inside a quartz ampule and four passive SiC TMs.

Figure 15 shows the assembly of the lower holder, lower spacer, upper holder, and upper spacer. First, the passive instrumentation was installed inside each holder or spacer. Then, WEC's temperature sensor was installed in the lower holder. The lower spacer, upper holder, upper spacer, and all centering thimbles were then slid over the MI cables from WEC's temperature sensor. At this point, the lower holder, lower spacer, and upper spacer assemblies were secured by using threaded rods and nuts. WEC's pressure sensor was assembled inside the upper holder, and its leads (i.e., MI cables and high-pressure gas line) passed up through the upper spacer; this was similar to the process performed to assemble the temperature sensor inside the lower holder. The upper holder was also secured with threaded rods and fasteners. The SPNDs were then placed inside their intended holders or spacers after passing through all holders or spacers located above the termination of each SPND. At this point, the MI cables for WEC's sensors and the SPNDs and the high-pressure gas line could be passed up through the experiment housing; compression fitting, including the internal sealant; hoses; Y-adapter; and the experiment junction box. It was necessary to pass these components upward through the experiment because the larger diameter of WEC's sensors and the SPND emitter regions could not fit through the compression seal. However, the gas lines, thermocouples, and fiber-optic sensor sheaths could be slid downward from the experiment junction box to where each component terminated within its designated holder or spacer.

Figure 15. Ordered (clockwise from top left) assembly of the lower holder, lower spacer, upper holder, and upper spacer.

The rupture disk assembly was already welded to the lower housing tube at this point. Similarly, the compression fitting body was already welded to the upper housing assembly, which included the lifting lugs and the o-ring seal where the experiment will eventually seal to HFIR's quick opening hatch. The flow restrictor was also welded to the upper housing tube before installing the internal experiment components. After inserting all sensors and gas lines, the leads were placed through the sides of the shield plug and secured by tack welding stainless-steel foils, as shown in Figure 16a. Then, the upper housing tube was slid downward so that it butted up against the weld coupler and the lower housing tube. The upper housing tube was rotated until matching holes in the upper housing tube and the shield plug (visible in the center of the plug in Figure 16a) aligned. A stainless-steel pin was inserted through these holes to prevent the shield plug from sliding or rotating. At this point, the two housing tubes were welded to the weld coupler, the pin was welded inside the upper housing tube, and the upper housing tube was welded to the upper housing assembly. Finally, the sealant for the compression fitting in Figure 16c was passed down into the body of the compression fitting (Figure 16b), and the fitting was torqued per the manufacturer's specifications. Figure 16d shows the fitting after torquing, including the gasket that was installed to prevent water from accumulating above the fitting inside the hose. Before the hose was connected to the upper housing assembly using hose clamps, epoxy was used to ensure that any small leakage of gas through the compression fitting would not enter the hose.

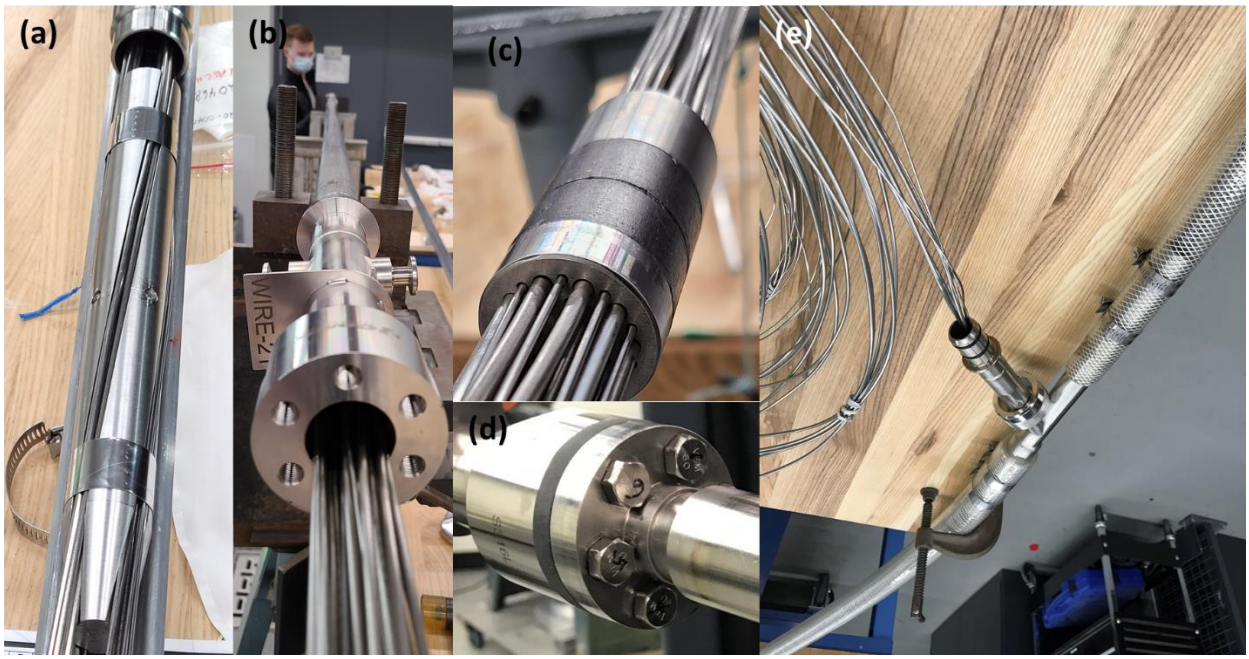

Figure 16. (a) Passing leads through the shield plug inside the experiment containment, (b) passing the leads through the top compression fitting, (c) sliding the compression sealant materials over all the leads, (d) the final sealed compression fitting, and (e) the gas lines splitting off from the sensor leads in the Y-adapter.

The opposite end of the hose was connected to the Y-adaptor via hose clamps. The gas lines were separated into one of the Y-adapter outlets (Figure 16e). The remaining sensor leads were passed through a second hose, which terminated at the experiment junction box, also via hose clamps. These connections are shown schematically in Figure 7b. The termination of the second hose at the experiment junction box is shown in Figure 17 on the left. Inside the experiment junction box, the MI cables were secured inside custom connectors via set screws, and the internal wires were soldered to bonding pads on the electronics board (Figure 17, top right). Tip, ring, and sleeve connectors were used to couple the board output to flexible triax cables. After making these connections, a platform was installed over the electronics board to allow the TCs and fiber optic sensors to connect to flexible cables. Figure 17 (top right) shows these connections. The TC and fiber sheaths were secured inside metal blocks with set screws. The TC wires were coupled to flexible TC extension wires via crimp connectors and heat shrink tubing. The fiber optic sensors were fusion spliced to fibers with Lucent connectors (LC) with an angled polish, referred to as *LC-APC*. Those splices were protected by using a plastic cover with adhesive. This allowed the flexible, connectorized fiber optic patch cables to be coupled to the experiment fibers inside the experiment junction box. All flexible cables were terminated with the appropriate pins that were installed inside Amphenol plugs. Figure 17 (left) shows how the flexible leads pass through outlet hoses before terminating inside Amphenol plugs, which are visible at the top left of Figure 17 and schematically shown in Figure 8.

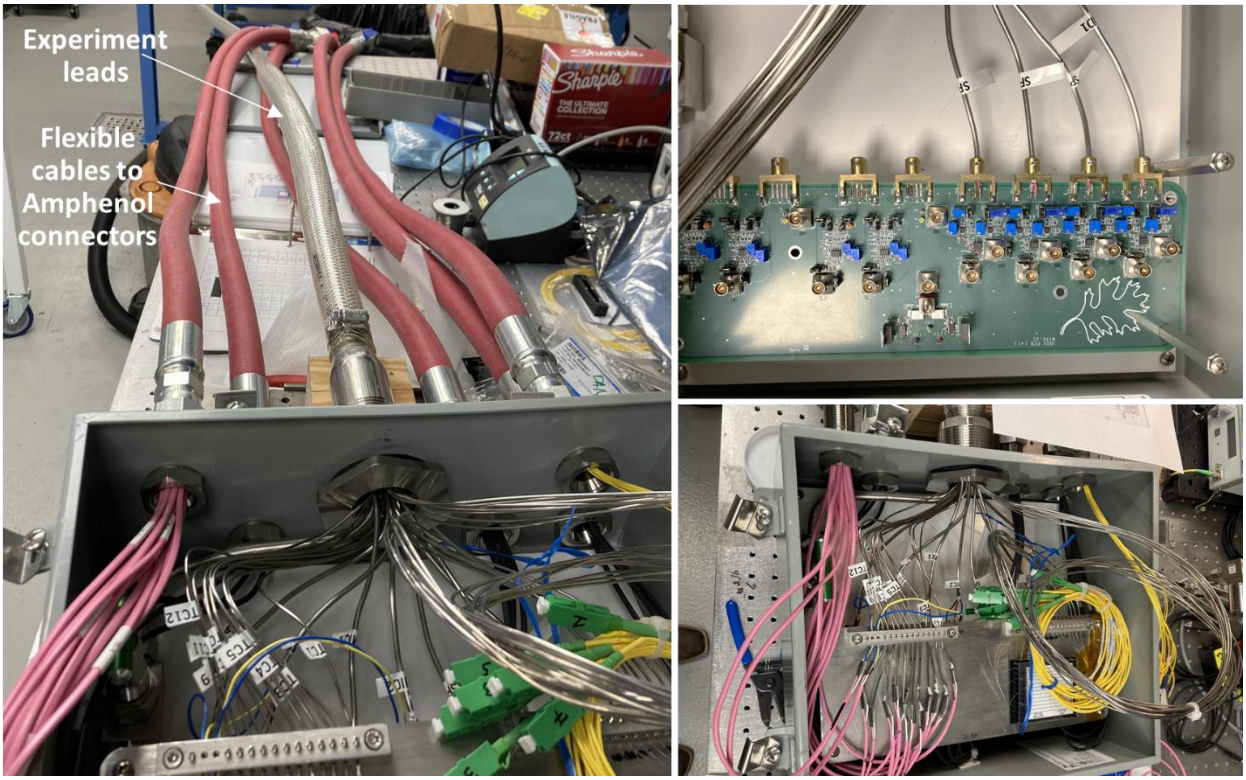

Figure 17. (Left) Passing the experiment leads into the experiment junction box and the flexible cables that pass through the outlet hoses to Amphenol connectors; (top right) the electronics board with the SPNDs terminated (WEC sensor terminations not shown); and (bottom right) the top layer of the experiment junction box where the fiber optic sensors and thermocouples transition to flexible cables.

The final step was to seal the outlet hoses with epoxy to allow the hose to be operated under a slight vacuum. This is necessary for checking for water leaks within the hose and for ensuring that any radioactive gases that may leak up through the sensor leads are swept through HFIR's off-gas monitoring system. In addition to sealing the outlet hoses, the main hose containing the sensor leads was also sealed in epoxy near the location where the leads enter the experiment junction box. However, an open-ended metal tube with a ball valve on one end (the end inside the junction box) was installed inside the hose before creating the epoxy seal. This valve (visible in the lower left of Figure 17 below the pink flexible cables) could be opened to pull vacuum inside the box, but it could also be closed during the experiment installation. This is necessary because the hose must be positively pressurized to check for bubbles, which would indicate a leak, before operation. The experiment junction box is not rated for positive pressure, so the valve prevents the box from becoming over-pressurized during testing. Figure 18 shows a full view of the entire assembled experiment before packaging for delivery to HFIR.

Figure 18. The final assembled experiment.

6.2 MIF AND CABLING MODIFICATIONS

Commercial junction boxes were mounted in the MIF (Figure 19) to provide convenient access for WEC's staff and future experiments that would target similar sensors that require fiber optic transmission or low-noise electrical cabling. LC/APC connectors were used inside the fiber optic junction box. The triax junction box uses bayonet nut coupling connectors. New cabling was installed from these junction boxes through HFIR's cable trays and the pool wall penetration (bottom right of Figure 2) and was terminated with Amphenol receptacles in the in-pool electrical junction box (bottom left of Figure 2).

Other modifications made for this experiment included upgrading the pressure rating for the high-pressure bellows supply gas line and adding cabling to enable convenient monitoring of a pressure transducer connected to the bellows supply gas line. A valved vacuum pump was also installed on the bellows supply gas line so that it could be evacuated and back-filled with He.

Figure 19. Fiber optic and triax junction boxes installed in the MIF.

6.3 NONDESTRUCTIVE EXAMINATIONS

After assembling, welding, and visually examining the welds, the experiment was subjected to a series of nondestructive examinations. First, He leak testing was performed on all welds, followed by hydrostatic testing at >7 MPa (~1,000 psi) and an additional series of He leak tests to ensure that the hydrostatic testing did not open any leaks. The welds were then tested by using a dye penetrant to ensure that there were no surface defects that might later result in a loss of hermeticity during operation. All welds and connections passed the required leak testing, hydrostatic testing, and dye penetrant testing. Additionally, the Conax compression seal passed the required He leak testing to ensure that there would not be significant quantities of gas leaking into the hose that contains the experiment leads during operation. Finally, the welds were examined for porosity via radiography. One weld showed a slight root concavity issue with an abrupt change in density. However, subsequent ultrasonic testing confirmed that the wall thickness in this region was sufficient to meet the American Society of Mechanical Engineers Boiler and Pressure Vessel Code. Therefore, these nondestructive tests collectively indicate that the experiment is acceptable for use. The detailed testing results are available upon request.

Additional radiographs were taken to ensure that the internal components did not move unexpectedly during welding or handling. Figure 20, Figure 21, and Figure 22 show radiographs of the lower holder, lower spacer, and upper holder regions, respectively. These radiographs show how the ICs, FS, and bellows within WEC's sensors are located where expected and that there are no indications that the wiring suffered any damage. This is consistent with electrical tests that were performed throughout the assembly process to ensure that there were no breaks, shorts, or other issues that would affect sensor performance. The TCs, fiber sheaths, and SPNDs also appear to be located at the proper elevations.

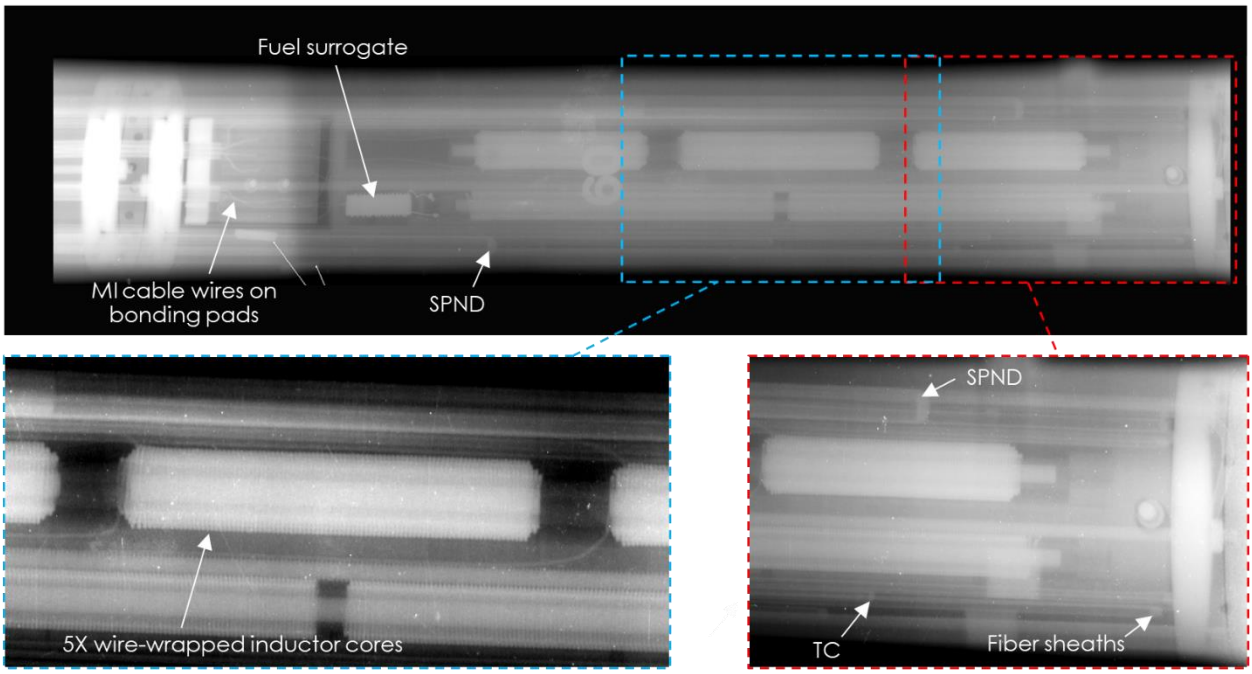

Figure 20. Radiographs of the lower holder and WEC's temperature sensor.

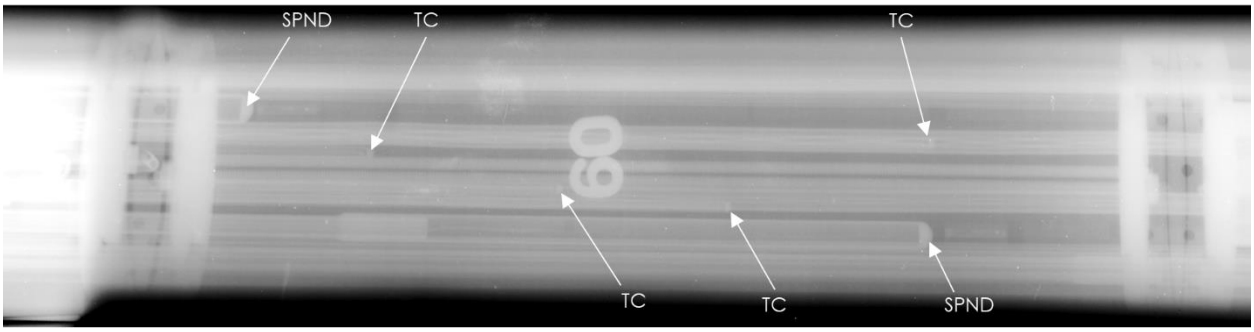

Figure 21. Radiographs of the lower spacer.

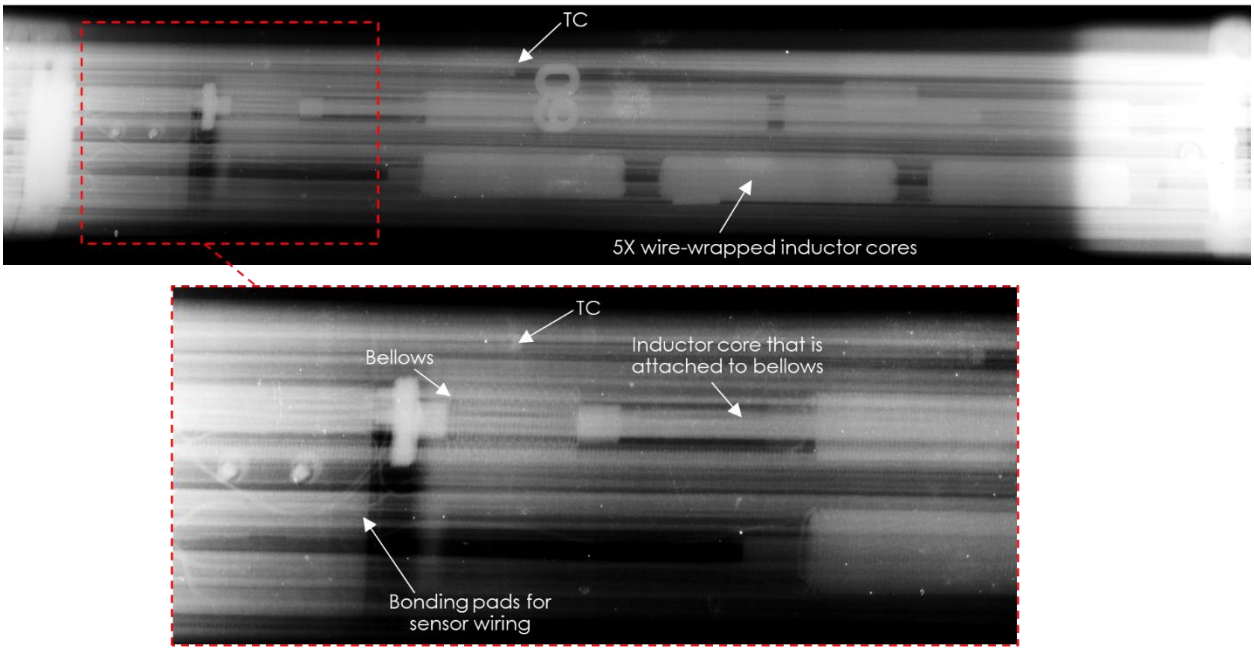

Figure 22. Radiographs of the upper holder and WEC's pressure sensor.

6.4 DELIVERY TO HFIR

The experiment was delivered to HFIR, installed within the reactor pool, and had its gas lines and sensors connected on February 17, 2022. The experiment is currently planned to begin reactor operation during HFIR cycle 498, which is scheduled to begin on April 5, 2022. Figure 23 shows photographs of the experiment being lowered into the pool and the sensor lead connections. The hoses and connections passed all leak testing, and all sensors appear to be functional following the installation.

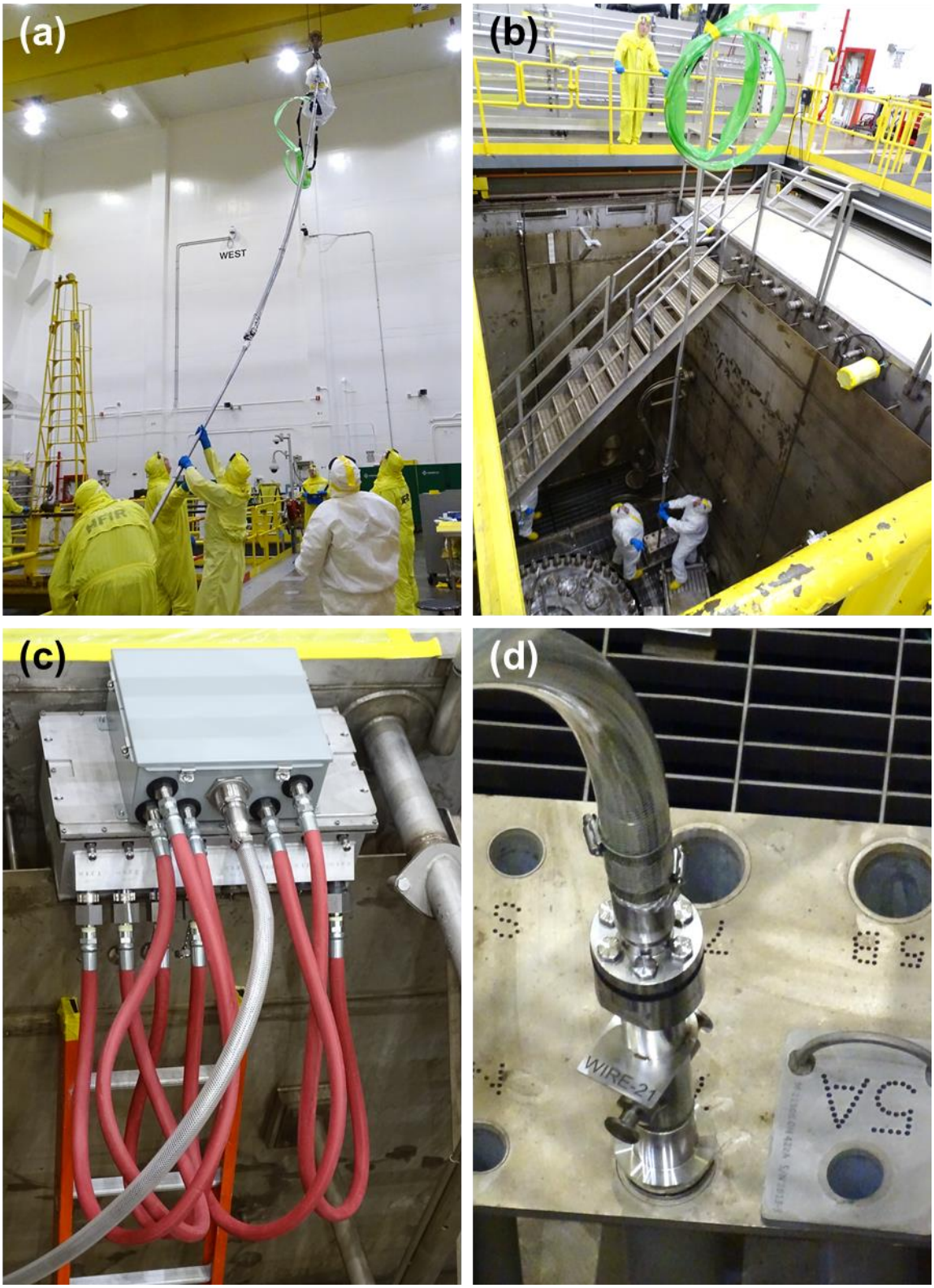

Figure 23. WIRE-21 installation into the HFIR pool and sensor lead connections.

Figure 24 shows the currently planned manipulations of the Ar concentration within the experiment, which determines the experiment temperatures, as well as the pressure within the bellows of WEC's pressure sensor. Data are shown vs. the time relative to the start of the first ~25 day HFIR cycle. The general plan is to first vary the Ar concentration in steps to determine how the sensor responds when the Curie point of the ICs is exceeded. Later, the pressure in the bellows will be increased in steps up to 300 psi to quantify the response of the sensor to known changes in pressure. Later in the cycle, the Ar concentration will again be cycled, followed by ramping up the pressure in steps to 400 psi. There may be some deviations from this plan based on how the sensors respond during the initial operation. Subsequent HFIR cycles will gradually increase the bellows pressure to higher values up to 800 psi.

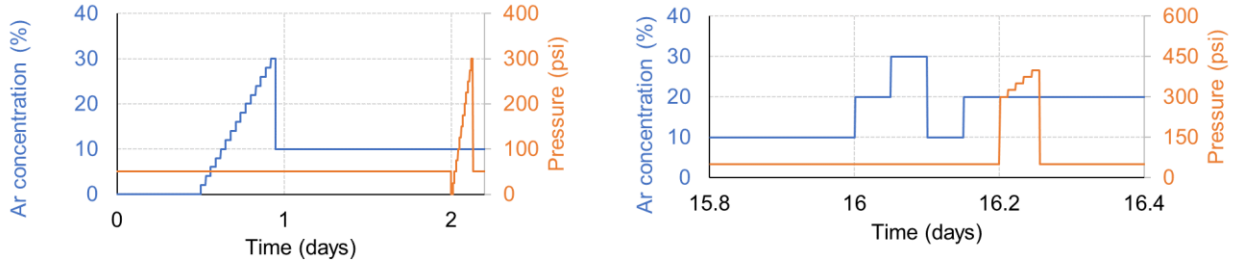

Figure 24. Planned manipulations of the Ar concentration within the experiment, which determines the experiment temperatures, and the pressure within the bellows of WEC's pressure sensor vs. time from the start of the first ~25 day HFIR cycle.

7. SUMMARY AND CONCLUSIONS

This report summarizes the objectives, design, analysis, assembly, testing, and delivery of a highly instrumented irradiation experiment designed to test WEC's wireless temperature and pressure sensors in HFIR. WEC's wireless sensors are being designed to provide in situ measurements of fuel centerline temperature and rod pressurization. This technology could provide valuable data for qualifying new fuels during irradiation in test reactors. Additionally, the wireless sensors could be deployed in operating commercial reactors to provide information to operators to reduce unnecessary conservatisms that are usually applied to fuel performance models, which do not take any credit for online measurements of fuel operating conditions. Before these wireless sensor technologies can be reliably deployed in either test reactors or commercial reactors, they must be tested to end-of-life neutron fluence levels and demonstrate acceptable performance. To this end, WIRE-21 will leverage HFIR's high neutron flux to perform accelerated testing on WEC's wireless sensors with in situ monitoring of the sensor response while subjecting the sensor to prototypic temperatures. In addition to WEC's sensors, the experiment is instrumented with many thermocouples, spatially distributed fiber optic temperature sensors, and passive temperature and neutron fluence monitors to provide detailed information regarding the temperature distribution within the experiment. This experiment will expose WEC's sensors to fast neutron fluences that are comparable to what might be accumulated during a full cycle of operation in a pressurized water reactor. If successful, the data collected from WEC's sensors could justify including these sensors in future lead test rods or lead test assemblies that contain accident tolerant fuels.

This is the most highly instrumented experiment ever conducted in HFIR. The in situ data collected from SPNDs and thermocouples will be invaluable for validating neutronic/thermal models and passive sensing techniques (e.g., SiC TMs, flux wires). This experiment will also test fiber optic sensors to higher neutron fluences than any previous study while simultaneously investigating different fiber dopants, Bragg gratings, and hollow core fibers. The improved cabling and connectors and the design of a compression fitting for passing instrument leads through the experiment pressure boundary will greatly simplify the ability to test similar sensors in future instrumented HFIR experiments.

8. REFERENCES

[1] J. Carvajal, S. Stafford, J. Arndt, P. Sirianni, M. Heagy, E. Tatli, D. Carpenter, Y. Ostrovsky, Integral Fuel Rod Real-Time Wireless Sensor, 11th International Conference On Nuclear Plant Instrumentation, Control, and Human-Machine Interface Technologies Orlando, FL, 2019, pp. 1000–1012.
[2] J. Carvajal, J. Arndt, S. Stafford, M. Heagy, J. Abel II, E. Tatli, Detection apparatus usable in a nuclear reactor, and associated method, in: U.S.P.a.T. Office (Ed.) Westinghouse Electric Company LLC, United States, 2020.
[3] R.D. Cheverton, T.M. Sims, HFIR Core Nuclear Design, Oak Ridge National Laboratory, Oak Ridge, TN, 1971.
[4] J.V. Carvajal, M.D. Heibel, N.G. Arlia, A. Bascom, K. Ünlü, Nuclear Radiation–Tolerant Wireless Transmitter Irradiation Test Results, Nucl. Technol. 197(2) (2017) 201–208.
[5] P.L. Mulligan, K. Smith, N.D.B. Ezell, D.C. Sweeney, K. Godsey, A. James, A.L. Coq, J. McDuffee, J. Carvajal, C.M. Petrie, Wireless Instrumented RB Experiment Preliminary Design and Analysis, Oak Ridge National Laboratory, Oak Ridge, TN, 2020.
[6] K. Sawa, T. Tobita, Investigation of Irradiation Behavior of SiC-Coated Fuel Particle at Extended Burnup, Nucl. Technol. 142(3) (2003) 250–259.
[7] K. Minato, K. Sawa, K. Fukuda, C.A. Baldwin, W.A. Gabbard, O.F. Kimball, C.M. Malone, F.C. Montgomery, B.F. Myers, P. N.H., HRB-22 capsule irradiation test for HTGR fuel (JAERI/USDOE collaborative irradiation test), Japan Atomic Energy Research Institute, Japan, 1998.
[8] F. Homan, E. Long Jr, R. Hamner, B. Montgomery, K. Valentine, M. Kania, Irradiation performance of HTGR fuel rods in HFIR experiments HRB-4 and-5, Oak Ridge National Laboratory, Oak Ridge, TN, 1976.
[9] K. Valentine, F. Homan, E. Long Jr, T. Tiegs, B. Montgomery, R. Hamner, R. Beatty, Irradiation performance of HTGR fuel rods in HFIR experiments HRB-7 and-8, Oak Ridge National Laboratory, Oak Ridge, TN, 1977.
[10] F. Homan, T. Tiegs, M. Kania, E. Long Jr, K. Thoms, J. Robbins, P. Wagner, Irradiation performance of HTGR fuel rods in HFIR experiments HRB-11 and-12, Oak Ridge National Laboratory, Oak Ridge, TN, 1980.
[11] N.O. Cetiner, G.L. Yoder, J.L. McDuffee, D. Wilder, Y.S. Kwon, C. Bryan, An advanced materials irradiation facility for materials and fuels irradiations at the high flux isotope reactor, Proceedings of Top Fuel 2016, Boise, ID, 2016, pp. 389–398.
[12] P.L. Mulligan, N.D.B. Ezell, K. Smith, K. Godsey, D. Sweeney, C. Petrie, J. Carvajal, S. Stafford, J. Arndt, In-Core Neutron Flux, Temperature, and Pressure Instrumentation for the WIRE-21 Experiment in the High Flux Isotope Reactor, 12th Nuclear Plant Instrumentation, Control and Human-Machine Interface Technologies, American Nuclear Society, United States, 2021, pp. 564-574.
[13] K.O. Hill, G. Meltz, Fiber Bragg grating technology fundamentals and overview, J. Lightw. Technol. 15(8) (1997) 1263–1276.
[14] D.C. Sweeney, A.M. Schrell, C.M. Petrie, An Adaptive Reference Scheme to Extend the Functional Range of Optical Backscatter Reflectometry in Extreme Environments, IEEE Sens. J. 21(1) (2020) 498–509.
[15] M. Froggatt, J. Moore, High-spatial-resolution distributed strain measurement in optical fiber with Rayleigh scatter, Appl. Opt. 37(10) (1998) 1735–1740.
[16] C.M. Petrie, A. Birri, T.E. Blue, High-dose temperature-dependent neutron irradiation effects on the optical transmission and dimensional stability of amorphous fused silica, J. Non-Cryst. Solids 525 (2019) 119668.
[17] G. Cheymol, H. Long, J.F. Villard, B. Brichard, High Level Gamma and Neutron Irradiation of Silica Optical Fibers in CEA OSIRIS Nuclear Reactor, IEEE Trans. Nucl. Sci. 55(4) (2008) 2252–2258.
[18] H.D. Warren, Calculational Model for Self-Powered Neutron Detector, Nucl. Sci. Eng. 48(3) (1972) 331–342.

[19] L.L. Snead, T. Nozawa, Y. Katoh, T.-S. Byun, S. Kondo, D.A. Petti, Handbook of SiC properties for fuel performance modeling, J. Nucl. Mater. 371(1–3) (2007) 329–377.
[20] K.G. Field, J.L. McDuffee, J.W. Geringer, C.M. Petrie, Y. Katoh, Evaluation of the continuous dilatometer method of silicon carbide thermometry for passive irradiation temperature determination, Nucl. Instr. Meth. Phys. Res. B 445 (2019) 46–56.
[21] J.M. Jacob, Industrial control electronics: applications and design, Prentice Hall1988.
[22] N. Xoubi, R.T. Primm III, Modeling of the High Flux Isotope Reactor Cycle 400, Oak Ridge, TN, 2005.
[23] C. Daily, S. Mosher, S.D. Wilson, D. Chandler, HFIRCON Version 1.0. 5 User Guide, Oak Ridge National Lab.(ORNL), Oak Ridge, TN (United States), 2020.

APPENDIX A. CALCULATED COMPONENT HEAT GENERATION RATES

Table A-1. Material-specific peak heat generation rates ($A_{m,d}$, W/g) for specific days of a HFIR cycle.
Results are shown for materials located in radial positions that face the HFIR core (core) and those that face the reflector (reflector).

Day of cycle	Al_2O_3, MgO, SiC, SiO_2		C	Ni, Inconel 600, V		Stainless-steel		W, Pt		Cu		Fe	
	Reflector	Core	All	Reflector	Core	Reflector	Core	Reflector	Core	Reflector	Core	Reflector	Core
0	7.06	9.70	8.32	8.38	10.81	11.12	12.61	16.08	20.40	10.19	12.03	8.18	11.23
1	7.54	10.28	8.70	9.39	12.51	11.97	13.77	17.59	22.01	11.13	13.68	9.04	12.14
3	7.58	10.31	8.73	9.61	13.06	11.49	13.28	17.73	22.40	12.04	13.66	9.21	12.08
5	7.60	10.36	8.73	9.63	12.81	11.18	13.02	17.86	22.62	11.65	13.80	9.10	12.34
10	7.66	10.43	8.79	10.17	13.19	10.84	12.65	18.22	22.68	11.69	14.04	9.26	12.32
15	7.80	10.54	8.90	10.63	13.87	10.90	12.76	18.53	23.96	12.28	14.76	9.57	12.67
20	7.99	10.81	9.06	11.41	15.00	11.42	13.07	19.51	24.30	12.53	14.69	9.85	13.04
22	7.98	10.89	9.10	11.44	15.19	11.50	13.28	19.31	25.04	12.46	14.77	10.03	13.16
24	8.14	11.02	9.21	11.88	15.62	11.84	13.86	19.95	25.10	12.61	15.42	10.13	13.54
26	8.20	11.01	9.23	12.23	16.05	11.98	13.90	20.34	25.15	12.62	15.48	10.24	13.63

Table A-2. HFIR heat generation rate spatial parameters (σ_d, cm) and peak location (z_{0_d}, cm) for specific days of a HFIR cycle.

Day of cycle	σ_d		z_{0_d}	
	Value	1 std	Value	1 std
0	25.29	0.74	0.13	0.26
1	25.22	0.80	-1.49	0.31
3	25.29	0.82	-1.75	0.27
5	25.36	0.74	-1.81	0.27
10	25.53	0.77	-1.97	0.26
15	25.46	0.82	-2.43	0.25
20	25.50	0.71	-3.43	0.27
22	25.80	0.78	-3.85	0.26
24	25.86	0.79	-4.41	0.38
26	26.45	0.73	-5.32	0.40

APPENDIX B. CALCULATED COMPONENT TEMPERATURES

Table B-1. Component average temperatures (in degrees Celsius) for day 1 of a HFIR cycle.

					Design point:	0	1	4	5	8	10
					Fill gas percent He:	100	70	100	70	85	85
					Heat generation rate radial position (C = core, R = reflector):	R	R	C	C	R	C
	Part	**Mat.**	**Mass (g)**	**T melt**							
Holder	Graphite.PS_Holder	POCO	199.52	3,650		188	247	208	273	218	242
Sensor housing	Al2O3.PS_Housing_1	Al_2O_3	73.416	2,054		210	281	242	323	246	284
	Al2O3.PS_Housing_2	Al_2O_3	103.27	2,054		246	324	286	377	286	332
	SS.PS_MI_Support	SS304	6.906	1,400		144	187	160	208	165	184
	Al2O3.PS_BondingPad	Al_2O_3	2.302	2,054		123	164	137	185	143	161
	SS.Bellows	SS304	0.625	1,400		146	195	166	222	170	194
	SS.BellowsTransition	SS304	0.741	1,400		150	201	169	228	176	199
	Fe.PS_Core.1.Top	Fe	0.053	1,535		207	268	244	315	238	280
	Fe.PS_Core.1	Fe	3.629	1,535		232	312	272	364	272	319
	Al2O3.PS_Insulation.1	Al_2O_3	4.531	2,054		254	340	299	397	298	349
	IW.PS_Wire.1a	Cu	1.556	1,083		207	279	241	324	244	283
	IW.PS_Wire.1b	Cu	1.973	1,083		204	275	237	319	240	279
	IW.PS_Wire.2a	Cu	1.554	1,083		282	377	331	439	331	386
	IW.PS_Wire.2b	Cu	1.973	1,083		280	373	327	434	327	382
	Fe.PS_Core.3	Fe	1.268	1,535		336	448	396	526	393	463
	Al2O3.PS_Insulation.3	Al_2O_3	1.466	2,054		328	438	387	513	384	452
	IW.PS_Wire.3a	Cu	1.174	1,083		322	429	379	501	377	442
	IW.PS_Wire.3b	Cu	1.448	1,083		319	424	375	495	373	437
	IW.PS_Wire.3c	Cu	1.757	1,083		315	417	370	488	367	431
	IW.PS_Wire.3d	Cu	2.027	1,083		309	409	363	478	360	422
	Al2O3.PS_Spacer3_4	Al_2O_3	0.114	2,054		304	409	360	481	357	422
	Fe.PS_Core.4	Fe	1.268	1,535		271	366	318	429	319	375
	Al2O3.PS_Insulation.4	Al_2O_3	1.513	2,054		267	361	314	422	314	369
	IW.PS_Wire.4a	Cu	1.178	1,083		261	351	306	411	307	359
	IW.PS_Wire.4b	Cu	1.448	1,083		258	347	302	405	303	355
	IW.PS_Wire.4c	Cu	1.76	1,083		255	341	298	399	299	350
	IW.PS_Wire.4d	Cu	2.027	1,083		250	335	293	391	293	343
	Al2O3.PS_Spacer4_5	Al_2O_3	0.114	2,054		240	325	282	381	283	333
	Fe.PS_Core.5	Fe	1.268	1,535		211	287	247	335	249	291
	Al2O3.PS_Insulation.5	Al_2O_3	1.552	2,054		210	285	245	332	248	289
	IW.PS_Wire.5a	Cu	1.179	1,083		206	278	239	323	242	281
	IW.PS_Wire.5b	Cu	1.448	1,083		203	274	236	318	239	278
	IW.PS_Wire.5c	Cu	1.757	1,083		201	270	233	313	236	274
	IW.PS_Wire.5d	Cu	2.027	1,083		197	264	229	307	231	269
	Al2O3.PS_Standoff	Al_2O_3	0.121	2,054		352	461	413	538	408	478
	SS.PS_Screw.1	SS304	0.112	1,400		122	163	136	183	143	160
	SS.PS_Screw.2	SS304	0.112	1,400		120	161	134	182	141	158
	SS.PS_Screw.3	SS304	0.366	1,400		375	481	439	558	430	501
Holder	Graphite.TS_Holder	POCO	233.40	3,650		185	217	204	240	201	222
Sensor housing	Al2O3.TS_Housing_1	Al_2O_3	73.199	2,054		229	288	268	338	259	304
	Al2O3.TS_Housing_2	Al_2O_3	103.06	2,054		271	340	323	404	306	364
Sensor components	Fuel.TS_FuelSurrogate	W	2.729	3,370		735	935	882	1,085	843	993
	Al2O3.FSResbond	Al_2O_3	0.163	2,054		709	904	845	1,045	815	956
	Pt.RTDCoil	Pt	0.673	1,768		687	879	814	1,012	792	924
	Al2O3.WireResbond	Al_2O_3	0.208	2,054		630	802	743	921	725	844
	SS.FS_TC	SS304	0.078	1,400		425	540	507	631	485	573
	SS.TS_MI_Support	SS304	6.906	1,400		405	475	463	538	441	502
	Al2O3.TS_BondingPad	Al_2O_3	2.302	2,054		278	348	324	403	314	364
	Fe.TS_Core.1	Fe	4.383	1,535		269	344	322	410	307	366
	Al2O3.TS_Insulation.1	Al_2O_3	3.964	2,054		268	341	320	407	304	364
	IW.TS_Wire.1a	Cu	1.687	1,083		284	360	339	429	322	385
	IW.TS_Wire.1b	Cu	2.177	1,083		279	351	333	419	315	377
	IW.TS_Wire.2a	Cu	1.687	1,083		236	301	279	356	268	318

				Design point:	0	1	4	5	8	10
				Fill gas percent He:	100	70	100	70	85	85
				Heat generation rate radial position (C = core, R = reflector):	R	R	C	C	R	C
	Part	**Mat.**	**Mass (g)**	**T melt**						
	IW.TS_Wire.2b	Cu	2.177	1,083	232	294	274	348	263	311
	Fe.TS_Core.3	Fe	1.314	1,535	275	361	328	431	318	380
	Al2O3.TS_Insulation.3	Al_2O_3	1.286	2,054	273	358	325	427	315	376
	IW.TS_Wire.3a	Cu	1.174	1,083	249	320	295	380	285	338
	IW.TS_Wire.3b	Cu	1.448	1,083	245	314	291	372	280	331
	IW.TS_Wire.3c	Cu	1.76	1,083	240	305	284	362	273	323
	IW.TS_Wire.3d	Cu	2.027	1,083	234	296	277	351	265	314
	Al2O3.TS_Spacer3_4	Al_2O_3	0.114	2,054	309	405	375	490	357	433
	Fe.TS_Core.4	FE	1.314	1,535	317	415	382	499	366	440
	Al2O3.TS_Insulation.4	Al_2O_3	1.345	2,054	315	412	379	495	364	438
	IW.TS_Wire.4a	Cu	1.175	1,083	287	368	344	440	328	392
	IW.TS_Wire.4b	Cu	1.446	1,083	283	362	339	432	323	386
	IW.TS_Wire.4c	Cu	1.757	1,083	277	351	331	420	314	376
	IW.TS_Wire.4d	Cu	2.026	1,083	269	339	322	406	304	364
	Al2O3.TS_Spacer4_5	Al_2O_3	0.114	2,054	353	461	431	560	407	496
	Fe.TS_Core.5	FE	1.314	1,535	352	459	426	553	406	490
	Al2O3.TS_Insulation.5	Al_2O_3	1.333	2,054	349	454	422	547	402	485
	IW.TS_Wire.5a	Cu	1.177	1,083	320	409	385	490	365	438
	IW.TS_Wire.5b	Cu	1.446	1,083	315	400	379	480	358	430
	IW.TS_Wire.5c	Cu	1.757	1,083	308	389	370	467	349	419
	IW.TS_Wire.5d	Cu	2.026	1,083	299	376	360	451	338	407
	Al2O3.TS_Standoff	Al_2O_3	0.977	2,054	238	309	281	365	274	323
	SS.TS_Screw.1	SS304	0.112	1,400	285	355	330	408	321	370
	SS.TS_Screw.2	SS304	0.112	1,400	263	330	305	381	297	344
	SS.TS_Screw.3	SS304	0.366	1,400	243	301	283	350	273	317
Thermocouple junctions	SS.TC1.Junc	SS304	0.085	1,400	123	164	135	181	144	158
	SS.TC2.Junc	SS304	0.085	1,400	167	218	187	245	193	217
	SS.TC3.Junc	SS304	0.085	1,400	240	281	258	303	261	281
	SS.TC4.Junc	SS304	0.085	1,400	220	259	238	279	240	259
	SS.TC5.Junc	SS304	0.085	1,400	221	259	238	279	240	259
	SS.TC6.Junc	SS304	0.085	1,400	230	269	249	290	249	270
	SS.TC7.Junc	SS304	0.085	1,400	251	325	285	366	289	327
	SS.TC8.Junc	SS304	0.085	1,400	193	256	218	288	225	254
	SS.TC9.Junc	SS304	0.085	1,400	178	208	200	233	193	217
	SS.TC10.Junc	SS304	0.085	1,400	179	211	201	237	195	220
	SS.TC11.Junc	SS304	0.085	1,400	187	222	209	247	205	228
	SS.TC12.Junc	SS304	0.085	1,400	219	255	250	289	237	270
Thermocouples (full length)	SS.TC1	SS304	0.787	1,400	127	169	136	181	148	159
	SS.TC2	SS304	1.121	1,400	135	178	147	194	157	171
	SS.TC3	SS304	3.142	1,400	210	261	232	287	236	261
	SS.TC4	SS304	2.466	1,400	208	263	231	291	236	262
	SS.TC5	SS304	2.692	1,400	208	262	231	289	236	261
	SS.TC6	SS304	2.917	1,400	209	261	231	288	236	260
	SS.TC7	SS304	1.788	1,400	161	211	179	233	186	206
	SS.TC8	SS304	1.454	1,400	138	184	151	201	161	177
	SS.TC9	SS304	4.821	1,400	203	249	224	273	227	249
	SS.TC10	SS304	4.488	1,400	188	235	206	256	212	232
	SS.TC11	SS304	3.821	1,400	185	234	201	254	210	228
	SS.TC12	SS304	4.154	1,400	201	248	220	271	225	247
MICs	SS.MIC1.Sheath	SS304	1.987	1,400	144	189	155	204	167	180
	MgO.MIC1.Insulation	MgO	0.895	2,800	144	189	155	205	167	181
	Cu.MIC1.W1	Cu	0.127	1,083	144	189	155	205	167	181
	Cu.MIC1.W2	Cu	0.127	1,083	144	189	156	205	167	181

				Design point:	0	1	4	5	8	10
				Fill gas percent He:	100	70	100	70	85	85
				Heat generation rate radial position (C = core, R = reflector):	R	R	C	C	R	C
	Part	**Mat.**	**Mass (g)**	**T melt**						
	Cu.MIC1.W3	Cu	0.127	1,083	144	189	156	205	167	181
	Cu.MIC1.W4	Cu	0.127	1,083	144	189	156	205	167	181
	SS.MIC2.Sheath	SS304	1.987	1,400	144	189	155	204	166	180
	MgO.MIC2.Insulation	MgO	0.895	2,800	144	189	155	205	167	180
	Cu.MIC2.W1	Cu	0.127	1,083	144	189	155	205	167	181
	Cu.MIC2.W2	Cu	0.127	1,083	144	189	155	205	167	181
	Cu.MIC2.W3	Cu	0.127	1,083	144	189	156	205	167	181
	Cu.MIC2.W4	Cu	0.127	1,083	144	189	155	205	167	181
	SS.MIC3.Sheath	SS304	12.057	1,400	215	269	236	294	242	265
	MgO.MIC3.Insulation	MgO	5.433	2,800	216	270	237	295	244	267
	Cu.MIC3.W1	Cu	0.768	1,083	217	271	238	297	245	268
	Cu.MIC3.W2	Cu	0.768	1,083	216	271	237	296	244	267
	Cu.MIC3.W3	Cu	0.768	1,083	216	270	237	296	244	267
	Cu.MIC3.W4	Cu	0.768	1,083	217	271	238	297	245	268
	SS.MIC4.Sheath	SS304	12.057	1,400	215	268	235	293	242	265
	MgO.MIC4.Insulation	MgO	5.433	2,800	216	270	237	295	243	266
	Cu.MIC4.W1	Cu	0.768	1,083	217	271	238	296	244	268
	Cu.MIC4.W2	Cu	0.768	1,083	216	271	237	296	244	268
	Cu.MIC4.W3	Cu	0.768	1,083	216	270	236	295	243	267
	Cu.MIC4.W4	Cu	0.768	1,083	216	270	237	295	244	267
SiC	SiC.TMP1	SiC(Irr)	0.326	2,400	139	185	153	204	162	179
	SiC.TMP2	SiC(Irr)	0.326	2,400	160	212	178	236	186	207
	SiC.TMP3	SiC(Irr)	0.326	2,400	185	245	207	274	215	241
	SiC.TMP4	SiC(Irr)	0.326	2,400	212	280	238	314	247	277
	SiC.TMP5	SiC(Irr)	0.326	2,400	241	317	271	355	280	315
	SiC.TMP6	SiC(Irr)	0.326	2,400	272	355	306	397	315	354
	SiC.TMP7	SiC(Irr)	0.326	2,400	314	401	353	447	360	403
	SiC.TMP8	SiC(Irr)	0.326	2,400	314	401	354	448	360	403
	SiC.TMP9	SiC(Irr)	0.326	2,400	273	356	308	399	316	355
	SiC.TMP10	SiC(Irr)	0.326	2,400	241	317	271	355	280	315
	SiC.TMP11	SiC(Irr)	0.326	2,400	211	279	238	313	246	277
	SiC.TMP12	SiC(Irr)	0.326	2,400	184	244	207	274	215	241
	SiC.TMP13	SiC(Irr)	0.326	2,400	159	211	177	236	186	207
	SiC.TMP14	SiC(Irr)	0.326	2,400	139	185	153	204	162	179
	SiC.TMM1	SiC(Irr)	0.326	2,400	232	283	256	314	258	285
	SiC.TMM2	SiC(Irr)	0.326	2,400	227	278	251	308	253	280
	SiC.TMM3	SiC(Irr)	0.326	2,400	236	288	261	320	262	291
	SiC.TMM4	SiC(Irr)	0.326	2,400	247	301	273	334	275	304
	SiC.TMM5	SiC(Irr)	0.326	2,400	282	341	311	376	312	345
	SiC.TMM6	SiC(Irr)	0.326	2,400	279	337	307	372	309	340
	SiC.TMM7	SiC(Irr)	0.326	2,400	245	299	270	331	272	301
	SiC.TMM8	SiC(Irr)	0.326	2,400	232	284	256	314	259	286
	SiC.TMM9	SiC(Irr)	0.326	2,400	224	275	247	304	250	276
	SiC.TMM10	SiC(Irr)	0.326	2,400	230	281	253	311	256	283
	SiC.TMT1	SiC(Irr)	0.326	2,400	263	315	298	357	289	328
	SiC.TMT2	SiC(Irr)	0.326	2,400	263	314	303	360	289	332
	SiC.TMT3	SiC(Irr)	0.326	2,400	246	295	282	338	271	311
	SiC.TMT4	SiC(Irr)	0.326	2,400	231	278	264	318	255	291
	SiC.TMT5	SiC(Irr)	0.326	2,400	215	259	245	296	237	271
	SiC.TMT6	SiC(Irr)	0.326	2,400	200	242	227	276	221	252
	SiC.TMT7	SiC(Irr)	0.326	2,400	204	246	230	278	225	254
	SiC.TMT8	SiC(Irr)	0.326	2,400	203	246	230	278	225	254
	SiC.TMT9	SiC(Irr)	0.326	2,400	204	246	232	281	225	257

					Design point:	0	1	4	5	8	10
					Fill gas percent He:	100	70	100	70	85	85
					Heat generation rate radial position (C = core, R = reflector):	R	R	C	C	R	C
	Part	Mat.	Mass (g)	T melt							
	SiC.TMT10	SiC(Irr)	0.326	2,400		219	264	251	302	242	277
	SiC.TMT11	SiC(Irr)	0.326	2,400		235	283	270	324	259	298
	SiC.TMT12	SiC(Irr)	0.326	2,400		250	299	287	344	275	316
	SiC.TMT13	SiC(Irr)	0.326	2,400		260	311	299	356	286	328
	SiC.TMT14	SiC(Irr)	0.326	2,400		257	309	290	349	284	321
SPNDs	Inc600.SPND1.Cable	Inconel	19.578	1,393		205	253	228	281	230	256
	Inc600.SPND2.Cable	Inconel	7.761	1,393		172	225	193	250	199	222
	Inc600.SPND3.Cable	Inconel	11.7	1,393		210	263	235	293	238	266
	Inc600.SPND4.Cable	Inconel	15.639	1,393		202	255	225	283	230	255
	Inc600.SPND1.Emitter	Inconel	3.693	1,393		192	227	217	256	210	237
	Inc600.SPND2.Emitter	Inconel	3.678	1,393		287	357	325	401	323	365
	Inc600.SPND3.Emitter	Inconel	3.696	1,393		229	271	250	296	250	274
	Inc600.SPND4.Emitter	Inconel	3.693	1,393		258	302	291	339	281	315
	Van.SPND1.EmitterWire	V	0.063	1,735		187	221	212	250	205	231
	Van.SPND2.EmitterWire	V	0.063	1,735		315	387	358	436	353	399
	Van.SPND3.EmitterWire	V	0.063	1,735		235	278	257	305	256	281
	Van.SPND4.EmitterWire	V	0.063	1,735		233	276	261	310	255	286
	MgO.SPND1.Insulation	MgO	1.925	2,800		189	223	213	252	206	233
	MgO.SPND2.Insulation	MgO	1.925	2,800		302	373	343	419	339	383
	MgO.SPND3.Insulation	MgO	1.925	2,800		233	276	255	302	254	279
	MgO.SPND4.Insulation	MgO	1.925	2,800		247	291	279	328	269	304
Flux wires	Quartz.FluxWireHolder.1	Quartz	0.188	1,710		168	198	187	221	183	204
	Van.FluxWire.1	V	0.067	1,735		191	235	217	269	213	243
	Quartz.FluxWireHolder.2	Quartz	0.188	1,710		224	264	244	287	245	266
	Van.FluxWire.2	V	0.067	1,735		251	306	278	340	279	310
	Quartz.FluxWireHolder.3	Quartz	0.188	1,710		252	296	275	322	274	299
	Van.FluxWire.3	V	0.067	1,735		284	347	316	387	316	352
	Quartz.FluxWireHolder.4	Quartz	0.188	1,710		215	252	243	284	234	264
	Van.FluxWire.4	V	0.067	1,735		247	303	283	348	275	316
Optical fiber sheath	SS.SF1	SS304	5.24	1,400		190	235	209	257	213	234
	SS.SF2	SS304	5.24	1,400		206	250	227	276	229	252
	SS.SF3	SS304	5.24	1,400		208	252	229	277	230	254
	SS.SF4	SS304	5.24	1,400		190	234	209	257	213	234
	SS.SF5	SS304	5.24	1,400		209	253	231	279	232	256
	SS.SF6	SS304	5.24	1,400		193	237	212	260	215	237
	SS.SF7	SS304	5.24	1,400		208	252	230	278	231	255
	SS.SF8	SS304	5.24	1,400		190	234	209	257	212	233
Gas lines	SS.HP1	SS304	0.785	1,400		152	194	164	211	173	188
	SS.G1	SS304	5.266	1,400		191	235	211	258	214	235
	SS.G1.Tip	SS304	0.072	1,400		312	362	346	401	337	374
	SS.G2	SS304	2.232	1,400		200	257	223	284	229	255
	SS.G2.Tip	SS304	0.072	1,400		502	583	560	643	544	603
	SS.P1	SS304	11.546	1,400		186	230	204	252	208	229
Upper spacer	Graphite.UpperSpacer	POCO	63.861	3,650		132	175	140	188	154	165
	SS.CentThimb.1	SS304	15.9	1,400		122	165	130	177	144	154
	SS.ThimbNut.1.1	SS304	0.138	1,400		125	169	133	181	147	157
	SS.ThimbNut.1.2	SS304	0.138	1,400		128	172	136	184	150	161
	SS.ThimbNut.1.3	SS304	0.138	1,400		124	167	132	179	146	156
	SS.ThimbNut.1.4	SS304	0.138	1,400		127	171	136	183	149	160
	SS.TieRod.1.1	SS304	1.311	1,400		132	176	141	189	155	166
	SS.TieRod.1.2	SS304	1.311	1,400		134	180	144	193	157	169
	SS.TieRod.1.3	SS304	1.311	1,400		131	176	140	189	154	165
	SS.TieRod.1.4	SS304	1.311	1,400		133	178	142	191	156	167

				Design point:	0	1	4	5	8	10
				Fill gas percent He:	100	70	100	70	85	85
				Heat generation rate radial position (C = core, R = reflector):	R	R	C	C	R	C
	Part	**Mat.**	**Mass (g)**	**T melt**						
	SS.CentThimb.2	SS304	15.89	1,400	135	179	145	193	158	169
	SS.ThimbNut.2.1	SS304	0.138	1,400	143	188	153	203	166	179
	SS.ThimbNut.2.2	SS304	0.138	1,400	144	189	155	204	167	180
	SS.ThimbNut.2.3	SS304	0.138	1,400	142	187	152	201	165	177
	SS.ThimbNut.2.4	SS304	0.138	1,400	141	185	151	199	163	176
Upper holder	SS.CentThimb.3	SS304	15.891	1,400	136	179	147	193	158	170
	SS.ThimbNut.3.1	SS304	0.138	1,400	130	171	140	185	151	163
	SS.ThimbNut.3.2	SS304	0.138	1,400	128	170	138	183	149	161
	SS.ThimbNut.3.3	SS304	0.138	1,400	132	174	142	187	153	165
	SS.TieRod.2.1	SS304	5.168	1,400	195	259	217	287	228	253
	SS.TieRod.2.2	SS304	5.168	1,400	194	258	213	284	226	249
	SS.TieRod.2.3	SS304	5.168	1,400	198	263	218	289	232	255
	SS.CentThimb.4	SS304	15.891	1,400	319	408	359	455	365	409
	SS.ThimbNut.4.1	SS304	0.138	1,400	337	426	375	471	383	425
	SS.ThimbNut.4.2	SS304	0.138	1,400	333	422	367	463	379	417
	SS.ThimbNut.4.3	SS304	0.138	1,400	328	413	362	453	372	410
Lower spacer	Graphite.LowerSpacer	POCO	223.917	3,650	200	239	216	256	220	237
	SS.CentThimb.5	SS304	15.891	1,400	245	300	267	326	273	297
	SS.ThimbNut.5.1	SS304	0.138	1,400	269	330	294	359	300	327
	SS.ThimbNut.5.2	SS304	0.138	1,400	254	309	277	336	282	307
	SS.ThimbNut.5.3	SS304	0.138	1,400	263	324	287	352	294	320
	SS.ThimbNut.5.4	SS304	0.138	1,400	264	319	288	347	292	318
	SS.TieRod.3.1	SS304	3.579	1,400	217	270	234	291	244	263
	SS.TieRod.3.2	SS304	3.579	1,400	220	273	237	293	247	266
	SS.TieRod.3.3	SS304	3.579	1,400	219	272	238	294	246	266
	SS.TieRod.3.4	SS304	3.579	1,400	227	280	245	302	253	274
	SS.CentThimb.6	SS304	15.891	1,400	294	354	320	384	325	353
	SS.ThimbNut.6.1	SS304	0.138	1,400	319	385	347	419	353	384
	SS.ThimbNut.6.2	SS304	0.138	1,400	306	365	333	396	336	365
	SS.ThimbNut.6.3	SS304	0.138	1,400	340	408	372	444	374	409
	SS.ThimbNut.6.4	SS304	0.138	1,400	331	393	361	428	363	395
Lower holder	SS.CentThimb.7	SS304	15.891	1,400	353	420	385	457	388	422
	SS.ThimbNut.7.1	SS304	0.138	1,400	318	379	348	413	350	381
	SS.ThimbNut.7.2	SS304	0.138	1,400	301	356	328	387	329	358
	SS.ThimbNut.7.3	SS304	0.138	1,400	328	389	359	425	359	393
	SS.TieRod.4.1	SS304	5.168	1,400	186	221	205	243	204	225
	SS.TieRod.4.2	SS304	5.168	1,400	188	223	206	244	206	225
	SS.TieRod.4.3	SS304	5.168	1,400	191	225	213	250	208	232
	SS.CentThimb.8	SS304	20.341	1,400	212	258	236	288	235	263
	SS.ThimbNut.8.1	SS304	0.138	1,400	218	264	241	291	242	267
	SS.ThimbNut.8.2	SS304	0.138	1,400	206	248	226	272	227	249
	SS.ThimbNut.8.3	SS304	0.138	1,400	231	278	256	309	255	283
Housing and rupture disk	Standoff	SS304	16.123	1,400	165	206	179	225	186	203
	RuptureDiskAdapter	SS304	30.179	1,400	74	76	78	80	75	79
	RuptureDiskUpperHousing	SS304	59.819	1,400	106	106	113	114	106	113
	RuptureDisk	SS304	1.395	1,400	140	140	151	151	140	151
	RuptureDiskLowerHousing	SS304	43.591	1,400	112	112	120	120	112	120
	Housing	SS304	1610.63	1,400	75	75	79	79	75	79

Table B-2. Component average temperatures (in degrees Celsius) for day 26 of a HFIR cycle.

					Design point:	2	3	6	7	9	11
					Fill gas percent He:	100	70	100	70	85	85
					Heat generation rate radial position (C = core, R = reflector):	R	R	C	C	R	C
	Part	**Mat.**	**Mass (g)**	**T Melt**							
Holder	Graphite.PS_Holder	POCO	199.52	3,650		174	229	191	251	202	222
Sensor housing	Al2O3.PS_Housing_1	Al_2O_3	73.416	2,054		196	262	224	300	230	262
	Al2O3.PS_Housing_2	Al_2O_3	103.27	2,054		228	301	263	347	265	305
	SS.PS_MI_Support	SS304	6.906	1,400		129	167	143	186	148	165
	Al2O3.PS_BondingPad	Al_2O_3	2.302	2,054		112	149	125	167	130	146
	SS.Bellows	SS304	0.625	1,400		134	179	151	202	157	177
	SS.BellowsTransition	SS304	0.741	1,400		137	183	153	206	160	179
	Fe.PS_Core.1.Top	Fe	0.053	1,535		192	248	223	288	220	256
	Fe.PS_Core.1	Fe	3.629	1,535		216	290	250	336	253	293
	Al2O3.PS_Insulation.1	Al_2O_3	4.531	2,054		237	317	275	368	278	322
	IW.PS_Wire.1a	Cu	1.556	1,083		192	259	221	297	226	259
	IW.PS_Wire.1b	Cu	1.973	1,083		189	254	217	292	222	255
	IW.PS_Wire.2a	Cu	1.554	1,083		264	353	306	408	310	358
	IW.PS_Wire.2b	Cu	1.973	1,083		262	349	303	404	306	354
	Fe.PS_Core.3	Fe	1.268	1,535		315	422	369	492	370	431
	Al2O3.PS_Insulation.3	Al_2O_3	1.466	2,054		308	412	360	480	361	421
	IW.PS_Wire.3a	Cu	1.174	1,083		302	403	352	468	354	411
	IW.PS_Wire.3b	Cu	1.448	1,083		299	398	348	462	350	406
	IW.PS_Wire.3c	Cu	1.757	1,083		295	392	343	455	345	400
	IW.PS_Wire.3d	Cu	2.027	1,083		290	384	337	446	338	392
	Al2O3.PS_Spacer3_4	Al_2O_3	0.114	2,054		284	383	332	447	334	390
	Fe.PS_Core.4	Fe	1.268	1,535		252	341	293	397	297	345
	Al2O3.PS_Insulation.4	Al_2O_3	1.513	2,054		249	336	289	390	293	340
	IW.PS_Wire.4a	Cu	1.178	1,083		243	328	282	379	286	331
	IW.PS_Wire.4b	Cu	1.448	1,083		240	323	278	374	282	327
	IW.PS_Wire.4c	Cu	1.76	1,083		237	318	274	368	278	322
	IW.PS_Wire.4d	Cu	2.027	1,083		233	312	269	361	273	316
	Al2O3.PS_Spacer4_5	Al_2O_3	0.114	2,054		223	302	258	350	262	305
	Fe.PS_Core.5	Fe	1.268	1,535		195	266	225	307	231	266
	Al2O3.PS_Insulation.5	Al_2O_3	1.552	2,054		194	263	224	304	229	264
	IW.PS_Wire.5a	Cu	1.179	1,083		190	257	219	296	224	257
	IW.PS_Wire.5b	Cu	1.448	1,083		188	253	216	291	221	254
	IW.PS_Wire.5c	Cu	1.757	1,083		186	249	213	287	218	250
	IW.PS_Wire.5d	Cu	2.027	1,083		182	244	209	281	213	245
	Al2O3.PS_Standoff	Al_2O_3	0.121	2,054		328	432	383	503	382	445
	SS.PS_Screw.1	SS304	0.112	1,400		112	148	124	166	129	144
	SS.PS_Screw.2	SS304	0.112	1,400		110	147	123	165	128	143
	SS.PS_Screw.3	SS304	0.366	1,400		346	446	403	517	397	462
Holder	Graphite.TS_Holder	POCO	233.40	3,650		207	243	226	266	225	246
Sensor housing	Al2O3.TS_Housing_1	Al_2O_3	73.199	2,054		263	330	308	387	297	348
	Al2O3.TS_Housing_2	Al_2O_3	103.06	2,054		319	398	377	472	359	424
Sensor components	Fuel.TS_FuelSurrogate	W	2.729	3,370		864	1,070	1,016	1,218	977	1,127
	Al2O3.FSResbond	Al_2O_3	0.163	2,054		827	1,030	966	1,166	939	1,077
	Pt.RTDCoil	Pt	0.673	1,768		797	997	925	1,124	908	1,037
	Al2O3.WireResbond	Al_2O_3	0.208	2,054		725	905	837	1,018	826	940
	SS.FS_TC	SS304	0.078	1,400		477	597	564	693	540	631
	SS.TS_MI_Support	SS304	6.906	1,400		411	481	474	552	447	513
	Al2O3.TS_BondingPad	Al_2O_3	2.302	2,054		287	359	337	420	324	378
	Fe.TS_Core.1	Fe	4.383	1,535		320	407	382	486	364	434
	Al2O3.TS_Insulation.1	Al_2O_3	3.964	2,054		316	402	377	480	360	428
	IW.TS_Wire.1a	Cu	1.687	1,083		326	412	388	491	369	440
	IW.TS_Wire.1b	Cu	2.177	1,083		320	402	381	480	361	430
	IW.TS_Wire.2a	Cu	1.687	1,083		289	367	341	435	328	388

				Design point:	2	3	6	7	9	11
				Fill gas percent He:	100	70	100	70	85	85
				Heat generation rate radial position (C = core, R = reflector):	R	R	C	C	R	C
	Part	**Mat.**	**Mass (g)**	**T Melt**						
	IW.TS_Wire.2b	Cu	2.177	1,083	283	358	335	424	321	380
	Fe.TS_Core.3	Fe	1.314	1,535	343	449	409	536	396	472
	Al2O3.TS_Insulation.3	Al_2O_3	1.286	2,054	339	444	405	530	391	467
	IW.TS_Wire.3a	Cu	1.174	1,083	309	397	367	471	353	419
	IW.TS_Wire.3b	Cu	1.448	1,083	304	389	361	462	347	411
	IW.TS_Wire.3c	Cu	1.76	1,083	297	378	353	449	338	401
	IW.TS_Wire.3d	Cu	2.027	1,083	289	365	344	435	328	389
	Al2O3.TS_Spacer3_4	Al_2O_3	0.114	2,054	380	496	461	601	438	530
	Fe.TS_Core.4	FE	1.314	1,535	378	494	455	593	436	523
	Al2O3.TS_Insulation.4	Al_2O_3	1.345	2,054	376	490	452	588	433	520
	IW.TS_Wire.4a	Cu	1.175	1,083	342	437	408	522	390	465
	IW.TS_Wire.4b	Cu	1.446	1,083	336	429	402	512	383	457
	IW.TS_Wire.4c	Cu	1.757	1,083	328	416	393	498	373	445
	IW.TS_Wire.4d	Cu	2.026	1,083	319	401	381	481	361	431
	Al2O3.TS_Spacer4_5	Al_2O_3	0.114	2,054	414	538	504	653	476	578
	Fe.TS_Core.5	FE	1.314	1,535	402	522	484	628	462	556
	Al2O3.TS_Insulation.5	Al_2O_3	1.333	2,054	398	516	479	621	457	549
	IW.TS_Wire.5a	Cu	1.177	1,083	364	463	436	554	414	495
	IW.TS_Wire.5b	Cu	1.446	1,083	358	454	429	543	406	486
	IW.TS_Wire.5c	Cu	1.757	1,083	350	441	419	528	396	473
	IW.TS_Wire.5d	Cu	2.026	1,083	339	425	407	510	383	459
	Al2O3.TS_Standoff	Al_2O_3	0.977	2,054	297	384	351	454	341	403
	SS.TS_Screw.1	SS304	0.112	1,400	292	364	341	424	329	383
	SS.TS_Screw.2	SS304	0.112	1,400	272	341	319	398	308	359
	SS.TS_Screw.3	SS304	0.366	1,400	306	377	359	443	342	401
Thermocouple junctions	SS.TC1.Junc	SS304	0.085	1,400	114	151	124	164	132	144
	SS.TC2.Junc	SS304	0.085	1,400	154	201	171	223	178	197
	SS.TC3.Junc	SS304	0.085	1,400	238	279	252	296	259	274
	SS.TC4.Junc	SS304	0.085	1,400	208	245	221	260	227	241
	SS.TC5.Junc	SS304	0.085	1,400	212	249	225	264	231	244
	SS.TC6.Junc	SS304	0.085	1,400	225	263	239	279	244	259
	SS.TC7.Junc	SS304	0.085	1,400	234	304	263	339	270	302
	SS.TC8.Junc	SS304	0.085	1,400	179	238	200	265	209	233
	SS.TC9.Junc	SS304	0.085	1,400	211	247	236	276	229	256
	SS.TC10.Junc	SS304	0.085	1,400	203	240	228	269	222	248
	SS.TC11.Junc	SS304	0.085	1,400	198	234	220	259	217	240
	SS.TC12.Junc	SS304	0.085	1,400	244	283	276	319	264	298
Thermocouples (full length)	SS.TC1	SS304	0.787	1,400	116	153	123	163	134	143
	SS.TC2	SS304	1.121	1,400	124	162	133	175	143	154
	SS.TC3	SS304	3.142	1,400	196	243	214	265	220	240
	SS.TC4	SS304	2.466	1,400	191	242	211	266	217	239
	SS.TC5	SS304	2.692	1,400	193	242	211	264	218	238
	SS.TC6	SS304	2.917	1,400	194	242	212	264	219	239
	SS.TC7	SS304	1.788	1,400	148	194	163	212	171	188
	SS.TC8	SS304	1.454	1,400	127	168	138	183	148	160
	SS.TC9	SS304	4.821	1,400	201	245	220	267	223	244
	SS.TC10	SS304	4.488	1,400	183	227	198	246	205	223
	SS.TC11	SS304	3.821	1,400	175	221	189	238	199	214
	SS.TC12	SS304	4.154	1,400	194	238	210	258	216	235
MICs	SS.MIC1.Sheath	SS304	1.987	1,400	130	169	139	182	150	161
	MgO.MIC1.Insulation	MgO	0.895	2,800	130	169	139	183	150	161
	Cu.MIC1.W1	Cu	0.127	1,083	130	170	139	183	150	161
	Cu.MIC1.W2	Cu	0.127	1,083	130	170	139	183	150	161

				Design point:	2	3	6	7	9	11
				Fill gas percent He:	100	70	100	70	85	85
				Heat generation rate radial position (C = core, R = reflector):	R	R	C	C	R	C
	Part	**Mat.**	**Mass (g)**	**T Melt**						
	Cu.MIC1.W3	Cu	0.127	1,083	130	170	139	183	150	161
	Cu.MIC1.W4	Cu	0.127	1,083	130	170	139	183	150	161
	SS.MIC2.Sheath	SS304	1.987	1,400	129	169	139	182	150	161
	MgO.MIC2.Insulation	MgO	0.895	2,800	130	169	139	183	150	161
	Cu.MIC2.W1	Cu	0.127	1,083	130	169	139	183	150	161
	Cu.MIC2.W2	Cu	0.127	1,083	130	170	139	183	150	161
	Cu.MIC2.W3	Cu	0.127	1,083	130	170	139	183	150	161
	Cu.MIC2.W4	Cu	0.127	1,083	130	170	139	183	150	161
	SS.MIC3.Sheath	SS304	12.057	1,400	203	254	221	275	229	248
	MgO.MIC3.Insulation	MgO	5.433	2,800	204	255	222	277	230	250
	Cu.MIC3.W1	Cu	0.768	1,083	205	256	223	278	231	251
	Cu.MIC3.W2	Cu	0.768	1,083	205	256	222	278	231	250
	Cu.MIC3.W3	Cu	0.768	1,083	204	255	222	277	230	250
	Cu.MIC3.W4	Cu	0.768	1,083	205	256	223	278	231	251
	SS.MIC4.Sheath	SS304	12.057	1,400	203	253	220	274	228	248
	MgO.MIC4.Insulation	MgO	5.433	2,800	204	255	222	276	230	249
	Cu.MIC4.W1	Cu	0.768	1,083	205	256	223	278	231	251
	Cu.MIC4.W2	Cu	0.768	1,083	205	255	222	277	231	250
	Cu.MIC4.W3	Cu	0.768	1,083	204	255	222	277	230	250
	Cu.MIC4.W4	Cu	0.768	1,083	204	255	222	277	230	250
SiC	SiC.TMP1	SiC(Irr)	0.326	2,400	128	169	139	185	149	162
	SiC.TMP2	SiC(Irr)	0.326	2,400	147	194	161	214	171	188
	SiC.TMP3	SiC(Irr)	0.326	2,400	170	225	188	249	198	219
	SiC.TMP4	SiC(Irr)	0.326	2,400	196	259	217	287	228	253
	SiC.TMP5	SiC(Irr)	0.326	2,400	223	294	248	327	260	289
	SiC.TMP6	SiC(Irr)	0.326	2,400	253	332	282	368	294	327
	SiC.TMP7	SiC(Irr)	0.326	2,400	292	374	326	415	335	373
	SiC.TMP8	SiC(Irr)	0.326	2,400	293	375	327	416	335	373
	SiC.TMP9	SiC(Irr)	0.326	2,400	254	333	283	369	295	328
	SiC.TMP10	SiC(Irr)	0.326	2,400	223	295	249	327	260	289
	SiC.TMP11	SiC(Irr)	0.326	2,400	195	258	216	286	227	252
	SiC.TMP12	SiC(Irr)	0.326	2,400	170	225	188	249	198	219
	SiC.TMP13	SiC(Irr)	0.326	2,400	147	194	161	214	170	187
	SiC.TMP14	SiC(Irr)	0.326	2,400	128	169	139	185	149	162
	SiC.TMM1	SiC(Irr)	0.326	2,400	220	269	240	295	245	268
	SiC.TMM2	SiC(Irr)	0.326	2,400	219	269	239	294	244	266
	SiC.TMM3	SiC(Irr)	0.326	2,400	231	282	251	309	257	280
	SiC.TMM4	SiC(Irr)	0.326	2,400	246	300	267	328	273	298
	SiC.TMM5	SiC(Irr)	0.326	2,400	283	342	309	374	313	342
	SiC.TMM6	SiC(Irr)	0.326	2,400	279	338	304	369	309	337
	SiC.TMM7	SiC(Irr)	0.326	2,400	243	297	263	324	270	294
	SiC.TMM8	SiC(Irr)	0.326	2,400	227	278	246	303	253	274
	SiC.TMM9	SiC(Irr)	0.326	2,400	216	265	234	289	241	262
	SiC.TMM10	SiC(Irr)	0.326	2,400	218	267	237	292	243	265
	SiC.TMT1	SiC(Irr)	0.326	2,400	281	336	314	376	309	346
	SiC.TMT2	SiC(Irr)	0.326	2,400	289	344	328	389	317	359
	SiC.TMT3	SiC(Irr)	0.326	2,400	275	330	311	373	303	343
	SiC.TMT4	SiC(Irr)	0.326	2,400	265	318	299	359	292	330
	SiC.TMT5	SiC(Irr)	0.326	2,400	253	304	285	343	279	315
	SiC.TMT6	SiC(Irr)	0.326	2,400	241	291	271	328	266	300
	SiC.TMT7	SiC(Irr)	0.326	2,400	250	301	281	339	276	310
	SiC.TMT8	SiC(Irr)	0.326	2,400	250	301	281	339	276	310
	SiC.TMT9	SiC(Irr)	0.326	2,400	246	296	278	335	272	307

				Design point:	2	3	6	7	9	11
				Fill gas percent He:	100	70	100	70	85	85
				Heat generation rate radial position (C = core, R = reflector):	R	R	C	C	R	C
	Part	**Mat.**	**Mass (g)**	**T Melt**						
	SiC.TMT10	SiC(Irr)	0.326	2,400	258	310	293	352	285	323
	SiC.TMT11	SiC(Irr)	0.326	2,400	271	325	307	368	298	338
	SiC.TMT12	SiC(Irr)	0.326	2,400	281	336	319	381	309	351
	SiC.TMT13	SiC(Irr)	0.326	2,400	286	340	323	385	313	355
	SiC.TMT14	SiC(Irr)	0.326	2,400	274	329	306	367	302	337
SPNDs	Inc600.SPND1.Cable	Inconel	19.578	1,393	203	251	223	276	228	251
	Inc600.SPND2.Cable	Inconel	7.761	1,393	161	210	178	233	186	206
	Inc600.SPND3.Cable	Inconel	11.7	1,393	199	249	221	276	225	250
	Inc600.SPND4.Cable	Inconel	15.639	1,393	195	247	216	272	222	245
	Inc600.SPND1.Emitter	Inconel	3.693	1,393	223	264	250	295	244	273
	Inc600.SPND2.Emitter	Inconel	3.678	1,393	270	337	303	376	305	341
	Inc600.SPND3.Emitter	Inconel	3.696	1,393	225	267	242	288	246	265
	Inc600.SPND4.Emitter	Inconel	3.693	1,393	275	322	308	359	299	334
	Van.SPND1.EmitterWire	V	0.063	1,735	220	261	247	292	241	270
	Van.SPND2.EmitterWire	V	0.063	1,735	297	366	335	410	333	375
	Van.SPND3.EmitterWire	V	0.063	1,735	232	276	251	298	254	274
	Van.SPND4.EmitterWire	V	0.063	1,735	249	297	278	331	273	304
	MgO.SPND1.Insulation	MgO	1.925	2,800	221	261	248	293	241	270
	MgO.SPND2.Insulation	MgO	1.925	2,800	284	352	320	394	320	359
	MgO.SPND3.Insulation	MgO	1.925	2,800	230	273	248	295	252	271
	MgO.SPND4.Insulation	MgO	1.925	2,800	265	312	296	349	289	323
Flux wires	Quartz.FluxWireHolder.1	Quartz	0.188	1,710	202	239	225	266	221	245
	Van.FluxWire.1	V	0.067	1,735	237	295	269	336	266	302
	Quartz.FluxWireHolder.2	Quartz	0.188	1,710	212	250	228	268	231	248
	Van.FluxWire.2	V	0.067	1,735	242	298	266	329	270	298
	Quartz.FluxWireHolder.3	Quartz	0.188	1,710	253	297	272	319	276	296
	Van.FluxWire.3	V	0.067	1,735	293	360	322	398	327	360
	Quartz.FluxWireHolder.4	Quartz	0.188	1,710	237	278	265	310	258	288
	Van.FluxWire.4	V	0.067	1,735	279	345	318	394	313	356
Optical fiber sheath	SS.SF1	SS304	5.24	1,400	190	233	206	253	212	230
	SS.SF2	SS304	5.24	1,400	206	250	225	273	229	249
	SS.SF3	SS304	5.24	1,400	208	251	227	274	230	251
	SS.SF4	SS304	5.24	1,400	190	233	206	253	212	230
	SS.SF5	SS304	5.24	1,400	210	254	231	278	232	254
	SS.SF6	SS304	5.24	1,400	193	236	211	258	215	235
	SS.SF7	SS304	5.24	1,400	209	253	230	277	232	254
	SS.SF8	SS304	5.24	1,400	190	233	207	254	212	231
Gas lines	SS.HP1	SS304	0.785	1,400	136	174	147	188	155	168
	SS.G1	SS304	5.266	1,400	192	235	210	256	214	233
	SS.G1.Tip	SS304	0.072	1,400	383	442	430	492	413	461
	SS.G2	SS304	2.232	1,400	184	236	203	259	211	232
	SS.G2.Tip	SS304	0.072	1,400	458	536	514	595	498	556
	SS.P1	SS304	11.546	1,400	186	229	202	249	208	226
Upper spacer	Graphite.UpperSpacer	POCO	63.861	3,650	120	158	127	168	139	148
	SS.CentThimb.1	SS304	15.9	1,400	112	149	118	159	131	139
	SS.ThimbNut.1.1	SS304	0.138	1,400	114	152	121	162	133	142
	SS.ThimbNut.1.2	SS304	0.138	1,400	116	155	123	165	136	144
	SS.ThimbNut.1.3	SS304	0.138	1,400	113	151	119	161	132	140
	SS.ThimbNut.1.4	SS304	0.138	1,400	116	154	123	164	135	144
	SS.TieRod.1.1	SS304	1.311	1,400	120	159	127	170	140	149
	SS.TieRod.1.2	SS304	1.311	1,400	122	162	129	172	142	151
	SS.TieRod.1.3	SS304	1.311	1,400	120	159	127	169	139	148
	SS.TieRod.1.4	SS304	1.311	1,400	121	161	128	171	141	150

				Design point:	2	3	6	7	9	11
				Fill gas percent He:	100	70	100	70	85	85
				Heat generation rate radial position (C = core, R = reflector):	R	R	C	C	R	C
	Part	**Mat.**	**Mass (g)**	**T Melt**						
	SS.CentThimb.2	SS304	15.89	1,400	122	161	130	172	142	152
	SS.ThimbNut.2.1	SS304	0.138	1,400	129	169	138	181	149	160
	SS.ThimbNut.2.2	SS304	0.138	1,400	129	169	138	182	150	160
	SS.ThimbNut.2.3	SS304	0.138	1,400	128	168	137	180	148	158
	SS.ThimbNut.2.4	SS304	0.138	1,400	127	166	135	178	147	157
Upper holder	SS.CentThimb.3	SS304	15.891	1,400	123	160	132	173	142	152
	SS.ThimbNut.3.1	SS304	0.138	1,400	118	154	126	166	136	146
	SS.ThimbNut.3.2	SS304	0.138	1,400	116	153	125	165	135	145
	SS.ThimbNut.3.3	SS304	0.138	1,400	120	156	128	168	138	148
	SS.TieRod.2.1	SS304	5.168	1,400	181	240	199	264	211	232
	SS.TieRod.2.2	SS304	5.168	1,400	179	238	195	260	209	228
	SS.TieRod.2.3	SS304	5.168	1,400	183	243	199	264	213	232
	SS.CentThimb.4	SS304	15.891	1,400	294	378	330	422	338	378
	SS.ThimbNut.4.1	SS304	0.138	1,400	310	394	345	437	354	393
	SS.ThimbNut.4.2	SS304	0.138	1,400	306	389	338	428	349	385
	SS.ThimbNut.4.3	SS304	0.138	1,400	301	381	332	418	342	377
Lower spacer	Graphite.LowerSpacer	POCO	223.917	3,650	195	233	207	246	214	227
	SS.CentThimb.5	SS304	15.891	1,400	226	279	246	302	253	275
	SS.ThimbNut.5.1	SS304	0.138	1,400	248	304	271	332	276	302
	SS.ThimbNut.5.2	SS304	0.138	1,400	234	286	255	310	260	283
	SS.ThimbNut.5.3	SS304	0.138	1,400	242	299	265	326	271	296
	SS.ThimbNut.5.4	SS304	0.138	1,400	243	295	265	321	269	293
	SS.TieRod.3.1	SS304	3.579	1,400	210	261	225	279	236	252
	SS.TieRod.3.2	SS304	3.579	1,400	213	263	226	281	238	254
	SS.TieRod.3.3	SS304	3.579	1,400	212	263	229	283	238	256
	SS.TieRod.3.4	SS304	3.579	1,400	219	270	234	289	245	262
	SS.CentThimb.6	SS304	15.891	1,400	292	352	318	382	323	351
	SS.ThimbNut.6.1	SS304	0.138	1,400	316	382	345	417	350	382
	SS.ThimbNut.6.2	SS304	0.138	1,400	304	362	330	393	334	362
	SS.ThimbNut.6.3	SS304	0.138	1,400	337	405	371	444	372	408
	SS.ThimbNut.6.4	SS304	0.138	1,400	328	390	358	426	360	392
Lower holder	SS.CentThimb.7	SS304	15.891	1,400	353	421	387	460	388	425
	SS.ThimbNut.7.1	SS304	0.138	1,400	320	381	351	417	351	385
	SS.ThimbNut.7.2	SS304	0.138	1,400	303	359	331	391	332	361
	SS.ThimbNut.7.3	SS304	0.138	1,400	329	391	363	430	361	397
	SS.TieRod.4.1	SS304	5.168	1,400	208	246	227	269	227	248
	SS.TieRod.4.2	SS304	5.168	1,400	209	248	226	268	229	247
	SS.TieRod.4.3	SS304	5.168	1,400	213	251	236	278	232	257
	SS.CentThimb.8	SS304	20.341	1,400	259	316	291	355	288	323
	SS.ThimbNut.8.1	SS304	0.138	1,400	266	322	295	356	294	326
	SS.ThimbNut.8.2	SS304	0.138	1,400	251	301	276	331	276	304
	SS.ThimbNut.8.3	SS304	0.138	1,400	282	340	316	380	311	348
Housing and rupture disk	Standoff	SS304	16.123	1,400	197	248	217	275	223	247
	RuptureDiskAdapter	SS304	30.179	1,400	82	84	87	89	83	88
	RuptureDiskUpperHousing	SS304	59.819	1,400	124	126	135	137	125	136
	RuptureDisk	SS304	1.395	1,400	171	171	188	189	171	189
	RuptureDiskLowerHousing	SS304	43.591	1,400	134	133	146	146	134	146
	Housing	SS304	1610.63	1,400	76	76	80	80	76	80